Scratch Detection on PCB using GMR Sensor

A Thesis

Submitted By

GAURAV CHANDRAKAR

for the award of the degree

of

MASTER OF TECHNOLOGY

Under the guidance of

Prof. Jagadeesh Kumar V

DEPARTMENT OF ELECTRICAL ENGINEERING

INDIAN INSTITUTE OF TECHNOLOGY MADRAS

May 2014

THESIS CERTIFICATE

This is to certify that the thesis titled **"Scratch detection on PCB using GMR Sensor",** submitted by **Mr. Gaurav Chandrakar**, to the Indian Institute of Technology Madras, Chennai for the award of the degree of **Master of Technology**, is a bona fide record of research work done by him under my supervision. The contents of this thesis, in full or a part has not been submitted to any other Institute or University for the award of any degree or diploma.

Dr. Jagadeesh Kumar V
Research Guide
Professor (CEC Head)
Dept. of Electrical Engineering
IIT-Madras, Chennai-600036

Place: Chennai
Date: 17 May 2014

ACKNOWLEDGEMENTS

I express my sincere and heartfelt gratitude to my guide, Dr. Jagadeesh Kumar V, Professor (CEC Head) for giving me this highly rewarding opportunity to work with him. His suggestions were sound and timely, which ensured the smooth progress of this work. His eye for detail, patience, meticulous nature, devotion to work is always a source of inspiration for me.

I am extremely grateful to Dr. Bobby George, Assistant Professor, Department of Electrical Engineering, IIT Madras, for his moral support and encouragement. His courses and insightful assignments helped me in understanding the finer aspects of Sensors and the instrumentation systems.

I thank all the teaching and non-teaching staff of the Department especially from Measurements and Instrumentation Lab and the department workshop, for their great help and also want to thank my friends Anand chandrashekhar, Md Suaib Danish, Piyush Kumar, Sachin sharma , Ritesh Pal Singh and Aniket Anil More for their timely assistance in the completion of this work.

Last but not the least, I would like to thank Almighty God, My parents and family for their support and for uncountable blessings due to which I was able to complete the project on time.

Gaurav Chandrakar

EE12M102

ABSTRACT

The inspection of defects on printed circuit boards (PCBs) by Giant magnetoresistive sensor (GMR) sensor and injecting current is proposed in this thesis. This technique is based on injecting AC currents through the metallic layer using two probes and detecting the perturbation of the magnetic field. An experiment was performed on a sample of rectangular piece of PCB to detect 3mm length of scratch which was located on the sample. The measurement was performed when the sensitive axis of GMR sensor is parallel to the scratch. The PCB sample was made of copper and the metal layer in this sample is about 100 microns in thickness. Two wires were soldered at the two ends of the rectangular sample. An AC current was supplied through these wires to the metal layer of the sample. By comparing the voltage output amplitude of the measurement conducted at each point , it was found that the there is a significant decrease in the output voltage as the sensor approaches the scratch and output voltage reaches the same level as it moves away from the proximity of scratch. Thus it is verified that scratch has been successfully detected. Applications of injecting current technique include detecting defects in thin metallic layers for IC manufacturing.

TABLE OF CONTENTS

LIST OF TABLES

LIST OF FIGURES

ABBREVIATIONS

AC	Alternating Current
GMR	Giant Magnetoresistance
DC	Direct Current
GND	Ground
PWM	Pulse Width Modulation
R	Resistance
AMR	Anisotropic Magnetoresistance
SDT	Spin Dependent Tunneling
MR	Magnetoresistance
PCB	Printed Circuit Board

CHAPTER 1
INTRODUCTION

1.1. Objective and scope of work

In this thesis, a Giant Magneto-Resistance (GMR) sensing system is introduced for detecting small defects in the order of hundreds of micrometers in length in thin films using injecting AC current method. The potential application of this technique is in IC manufacturing industry where it can be used for quality control of metallization layers on silicon wafers.

The GMR sensing system is also used in different detection techniques such as Eddy current testing and injecting current in various configurations. The GMR sensing system could also be used to measure non-uniform thickness for thin film coatings. The non-uniform thickness is due either to corrosion or cracking or some other deterioration.

The GMR testing method is called non destructive testing because the sample or specimen is not changed, damaged or destroyed during the testing and it can be used again. The GMR sensing system is capable of detecting small disruptive fields deeply flowing below or on the material surface. This system has an advantage of being capable of discovering defects in its early stage before it has grown where a failure can occur. The main industries that benefit from technique are airplane industry and nuclear power plants.

1.2. Organisation of work

This thesis is organized into five chapters, of which this is the first one. Chapter two provides a literature survey and an overview of magnetism and magnetic sensors. Several types of magnetoresistance (MR) were discussed such as Anisotropic Magneto resistance (AMR), Spin Dependent Tunnelling (SDT) and Giant magnetoresistance (GMR) .This part was mainly focused on GMR sensor, therefore, GMR theory was explained and GMR types were described (Spin valve GMR and Multilayer GMR). Chapter 3 gives the overview of the hardwares used in designing the system. It gives the detailed explanation of the components used along with their specifications and working. In chapter 4, designing of experimental testing system, its signal conditioning circuit and the working of whole system is discussed. Chapter 5 summarizes the results obtained followed by the conclusion of the work presented .Chapter 6 provides recommendations for future work .References and appendices are provided at the end of the thesis.

CHAPTER 2

LITERATURE SURVEY

The first section will discuss about magnetoresistance (MR), its types and applications. The second section will review GMR sensor theory and its applications. In addition, this chapter will discuss different types of magnetoresistance, including Anisotropic Magneto-Resistance (AMR), Giant magnetoresistance (GMR) and spin dependent tunneling (SDT).

The discovery of the Giant Magneto-Resistance (GMR) in 1988 was done by Peter Griinberg group, GMR was found in exchange coupling between two ferromagnetic layers separated by a nonmagnetic layer. The 2007 Nobel Prize in physics was awarded to Albert Fert and Peter Griinberg for the discovery of GMR. This invention opened the door to very important applications such as using GMR in magnetic nonvolatile memory and head read disk. In addition, the GMR sensor can be used for reading memory cells and to detect small defects in thin metallic structure.

2.1 Magneto-Resistance (MR)

Magneto-Resistance (MR) is the characteristic of a material that changes its electrical resistance when it is exposed to external magnetic field. G.Binasch defined the MR ratio in

1989 as the following equation:

$$MR\% = \frac{Rmax - Rmin}{Rmin}$$

Where,

R_{max} : Resistance of material without applying magnetic field

R_{min} : Resistance of material when magnetic field is applied

The Magneto-Resistance (MR) ratio represents the highest output voltage signal which is obtained from a magnetic sensor. The types of magnetoresistance sensors that will be discussed in this chapter include Anisotropic magnetoresistance (AMR), Spin dependent tunneling (SDT) and Giant magnetoresistance (GMR)[l-3].

2.1.1 Anisotropic Magneto-Resistance (AMR)

The Anisotropic Magneto-Resistance (AMR) existed in all ferromagnetic materials. AMR sensors are made of nickel-iron (Permalloy) thin film deposited on a silicon wafer and patterned in a resistive strip [4-5]. The thin film has its magnetic domains aligned along the long dimension of the sensor to make an "easy axis" orientation. Permalloy is a common material used for magnetic sensors because its characteristics are well-matched with the fabrication techniques used to make silicon integrated circuits and printed circuit board (PCBs).AMR is a quantum-mechanical effect and it was originally discovered by William Thomson [6]. The AMR is a result of electrons spin interactions of conduction electrons in the metal. The term "anisotropic" in AMR sensor refers to the fact that the resistance is a function of the angle created between the current and the magnetization directions [7-8]. Therefore, the change in resistivity in Permalloy film is a function of the angle ɵ between the magnetization (M) direction and the current (I) direction:

$$R = R_0 + \Delta R \cos^2 \theta$$

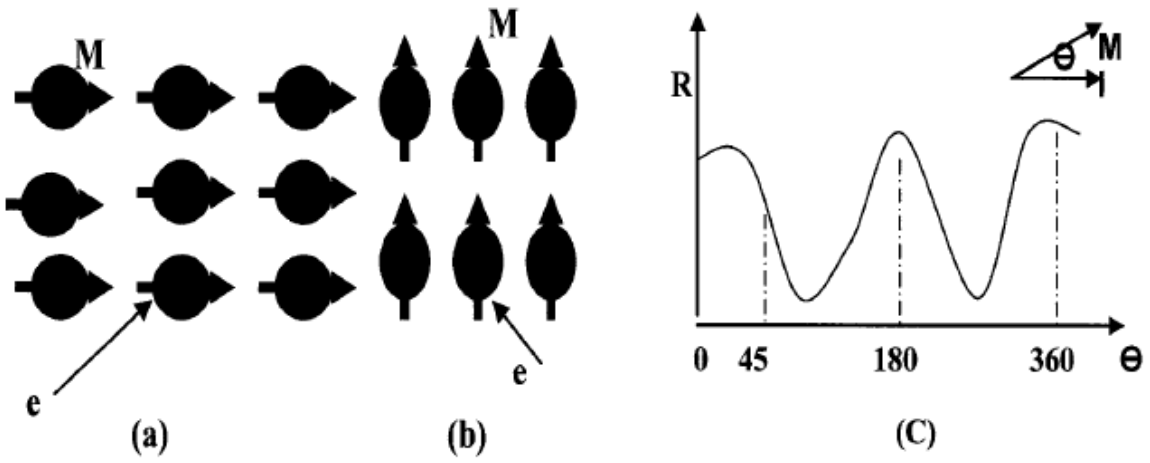

Fig 2.1.1.1 Demonstrating AMR Sensor effect

Figure 2.1.1.1 shows the electron orientations and the difference in scattering when magnetization orientation is parallel to the current direction (Figure 2.1.1.1 (a)) and perpendicular to the current direction (Figure 2.1.1.1 (b)). Resistance changes as a function of angle Ɵ between I and M as shown in (Figure 2.1.1.1(c)). AMR sensors have proven their stability in many applications [9]. AMR sensors used techniques to achieve low noise and high stability using flipping pulses of the sensor. These techniques can reduce non-linearity, hysteresis and temperature dependence. The AMR sensor device is used for many applications, such as high density read computer hard disk drives. Other applications include automotive wheel speed and crankshaft sensing, compass navigation, vehicle detection and current sensing [10].

2.1.2 Spin Dependent Tunneling (SDT)

SDT is also called Magnetic Tunnel Junctions (MTJ), which consists of two ferromagnetic layers separated by a thin insulating barrier layer. The ferromagnetic layers can be represented by magnetic electrodes. MTJs are important devices due to their potential applications, such as magnetic sensors and Magnetic Random Access Memories (MRAMs).The phenomenon of tunneling magnetoresistance (TMR) is a consequence of SDT. The TMR is due to an imbalance in the electric current carried by spin up and spin down electrons, which tunnels from a ferromagnetic layer to another layer through an insulator barrier. SDT was discovered by M.Julliere in 1975, then T.Niyazaki et al and by Moodera et al [11] discovered SDT independently in 1995. E.Y. Tsymbal et al.[12] studied the interface effects in spin-dependent tunneling and found that variations in the atomic potentials and bonding strengths near the interfaces have a profound effect resulting in the formation of interface resonant states, which dramatically affect the spin polarization and spin tunneling SDT junction is one of the promising technologies for sensor applications, such as in high density recording heads, magnetic memories and magnetic sensor arrays. The SDT devices have high TMR between 40 to 50% [13].

2.1.3 GMR sensor theory

GMR sensors have a higher sensitivity and a larger output signal compared to AMR sensors. The GMR sensor was introduced using Molt model in 1936. It showed a significant increase in resistivity on ferromagnetic materials when they are heated above Curie temperature. The electrical conductivity was demonstrated by Mott as two independent conducting channels, each channel has spin up electron and spin down electron. It explained that the scattering rates in metals are small compared to scattering rates in ferromagnetic materials. The GMR effect was first discovered in 1988 by Baibich *et al.* [12]. They studied the magnetoresistance of (001) Fe/(001) Cr sandwich structure and the spin dependent scattering of the electrons between the Fe and Cr layers. Figure 2.1.3.1 shows the hysteresis loops when the magnetic field was applied along [12] the layer plane for several (001)Fe/(001)Cr superlattices at 4.2 K. They proved that anitferromagnetic coupling between the adjacent Fe layers extremely increases when the Cr thickness decreases from 30 to 9**A.**

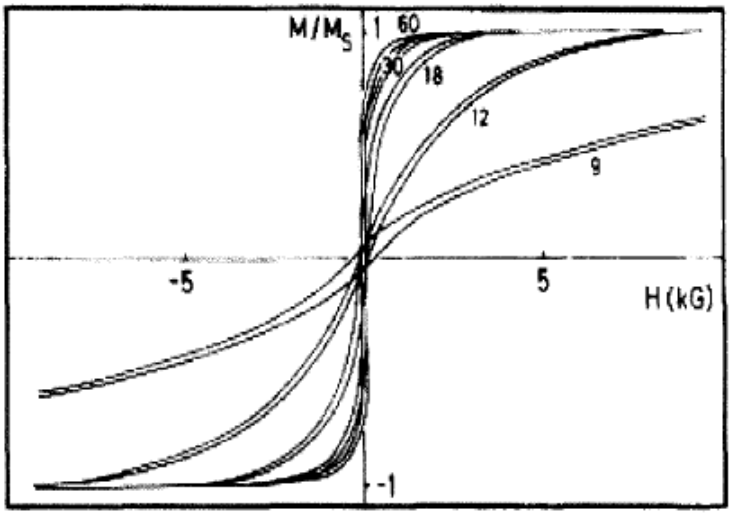

Fig 2.1.3.1 **:** Hysteresis loops for several (001)Fe/(001)Cr for different thickness of Cr and with presence of magnetic field by Baibich *et al.* [12].

Baibich *et al.* [12] investigated the Cr thickness and temperature dependency. They found that the magnetoresistance is lowered when the Cr thickness increases; therefore, the Anti Ferromagnetic (AF) coupling is weakened between the Fe layers as shown in Figure 2.1.3.2. By increasing the temperature from 4.2 K to room temperature, both the magnetoresistance

and *Hs* decrease, where *Hs* is the magnetic field needed to overcome the AF coupling and to saturate the magnetization. Two types of GMR will be discussed in this chapter, the first one is GMR spin valve and the second one is GMR multilayer.

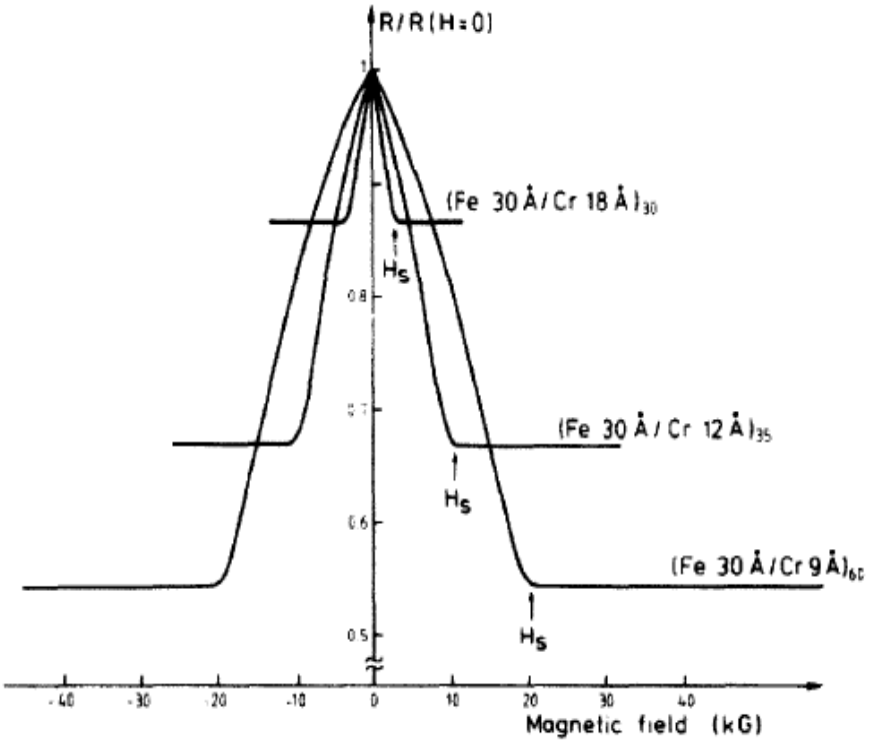

Fig 2.1.3.2: Magnetoresistance of three Fe/Cr super lattices at 4.2 k with different Cr thickness by Baibich *et al.* [12]

2.2 GMR Spin Valve

B. Dieny et al [13] introduced the term "spin valve magnetoresistance", which consists of two ferromagnetic layers separated by a thin non ferromagnetic material (NM). One of the two ferromagnetic layers has a fixed magnetization (hard layer). The other layer is called the soft layer, which is easy to manipulate by an external magnetic field. When coercive fields (Hc) of the ferromagnetic layers are different, it allows these layers to change their alignment from parallel to anti-parallel and vice versa. Therefore, the resistance alternates from low to high or from high to low based on the layer's orientation. The spin valve is due to the exchange

anisotropy, this phenomenon was first seen in the mid1950s in fine Co particles, covered by antiferromagnetic Co-oxide, but later it was reported in thin film structures. Dieny et al. [13] studied the exchange anisotropy, which is caused by the direct exchange between a ferromagnetic layer and adjoining antiferromagnetic layer in the GMR structure. They used two kinds of ferromagnetic materials with different coercivity. The free layer is easy to change its magnetization direction by magnetic field, on the other hand, the pinned layer has fixed to magnetization. On top of pinned layer, there is a pinning layer which needs high magnetic field to change its orientation and overcome the initial fixed field.

The physical origin of spin valve magnetoresistance can be explained using the two current model and the effects of GMR, which are summarized by Prinz [14]. He explained the effects of the GMR sensor as a result of the difference of the population in the conduction band for spin up and spin down electrons, which results from two reasons. The first reason is that the spin scattering occurs in any magnetic material, such as Fe or Co, because there is an imbalance of the spin populations at the Fermi level. Although, the density of states that is available to spin-up (majority electrons) and spin-down (minority electrons) are almost equal. However, the density of states is shifted in energy. This causes an uneven filling of the bands, which is the origin of the net magnetic moment for the materials. The second reason for the difference of the population in the conduction band will result from scattering spin up and spin down electrons when they encounter impurities and interfaces.

The principle of spin valve is explained based on electron orientations. First, in the case of the ferromagnetic layers have parallel magnetization directions, only one type of electrons (spin down) is scattered strongly, resulting in a relatively low resistivity of the material. On the other hand, when the magnetization of the layers are aligned antiparallel, both types of electrons (spin up and spin down) are scattered significantly, and thus the resistivity of the material is high.

In 1994, J. Daughton et al [15] designed and fabricated multilayered GMR sensor using Wheatstone bridge. The goal is to bias the sensor and get rid of the hysteresis effect and obtain linear output. The GMR bridge sensor consists of four resistors. Two resistors of the bridge sensor were shielded against magnetic field and concentrate the field on the other resistors. The two unshielded active resistors placed in the gap between two flux concentrators as shown in Figure 2.2.1. The sensitivity of a GMR bridge sensor can be adjusted in design by changing the lengths of the flux concentrators and the size of the gap between them. The purpose is to concentrate the magnetic field on the active magnetic

resistors to multiply the magnetic field and keep inactive resistors unchanged when the magnetic field is applied.

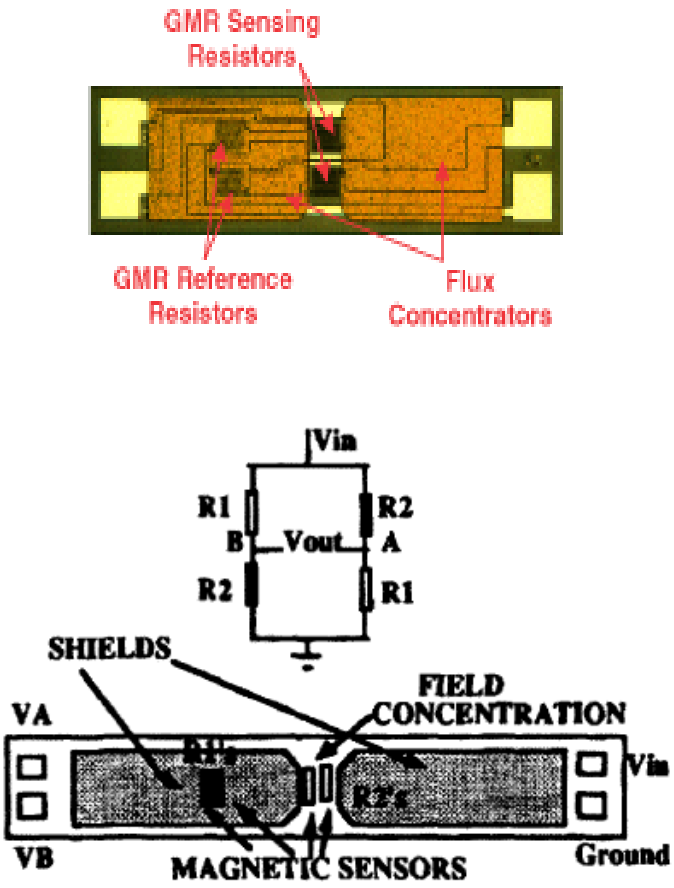

Figure 2.2.1: GMR Wheatstone bridge configurations with shielded resistor and multiplication field on active resistors, by J. Daughton *et al* [15].

N A. Stutzke et al [16] studied the low noise in the range from 0.1 Hz to 10 kHz for different commercially sensors including anisotropic magnetoresistance(AMR) giant magnetoresistance (GMR), and tunnel magnetoresistance (TMR). The following table summarized the sensor devices which, have been tested and compared in term of low frequency noise.

Sensor	Materials	Range (T)	Sensitivity (%/mT)	Resolution (μT)	Frequency (MHz)	Operating temperature & variation
Hall element	InSb, GaAs	10	-	1	0.01	-50 to +150 °C 2 %/°C
Anisotropic magneto-resistance	NiFe, FeCo	0.1	< 2	1	1	-50 to +150 °C 0.2 %/°C
Giant magneto-resistance	Magnetic/non-magnetic multi-layer film	1	< 2	1	> 100	-40 to +150 °C 0.09 %/°C
Spin-valve GMR	Magnetic/non-magnetic multi-layer film	0.01	< 200	0.01	> 100	-40 to +150 °C 0.09 %/°C
Magnetic impedance element	Amorphous material	0.001	< 1000	0.001	1	-40 to +125 °C

Table 2.2.1: Comparison Between Different Magnetic Sensors

The low field performance of all the measured sensors is compared in Figure 2.2.1 .The equivalent field noise or detectivity is shown at the DC bias field, which produces maximum sensitivity for each sensor. It can be seen that AMR type Honeywell HMC1001 has the lowest detectivity at frequencies below 100 Hz. In spite of GMR and TMR sensors devices have higher sensitivities; their intrinsic noise is higher, which give a higher low-field detectivity range. The higher noise of GMR and TMR sensors is because of their complex multilayer structure. In separate experiment, the measured voltage output and voltage noise at various frequencies versus applied magnetic field investigated of a NVE AAH002 GMR sensor. They found that the voltage signal noise increased when the sensitivity is high, that proves the presence of the magnetic noise component.

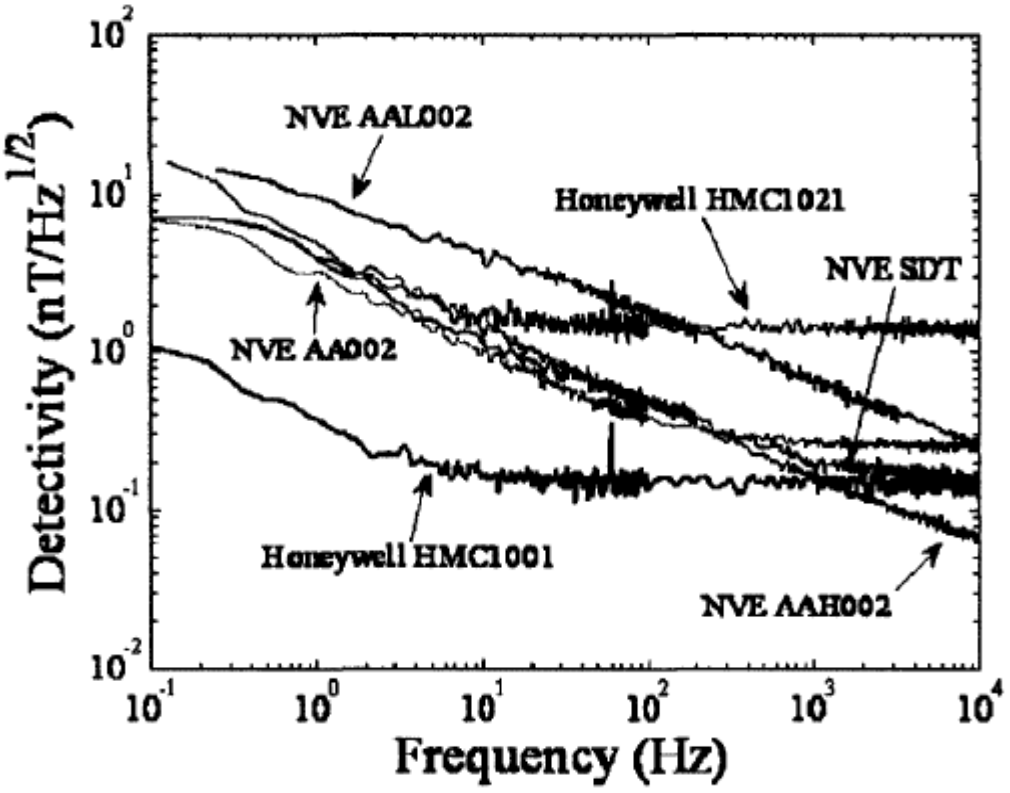

Fig 2.2.2 : Detectivity of several commercial sensors at dc magnetic bias field that produces highest sensitivity by N A. Stutzke *et al* [16]

2.3 GMR applications

The GMR can detect magnetic fields lower than Earth's which have found many applications in all major industries. There are several applications for devices based on GMR such as read heads for hard drives and Magnetic Random Access Memory (MRAM) [17-18]. GMR works as a testing device by itself as detecting defects on the surface of thin film. The GMR based Eddy current probe can detect defects on the surface and below the surface metallic structures. Magnetic sensors can also be used for moving traffic. One such application is the counting and classification of motor vehicles passing over portable or permanent sensors in the road. Another application is that by the use of arrays with two sensors; it can monitor the presence and speed of trains approaching road crossings in order to lower the crossing gates at the right time [19].

CHAPTER 3

HARDWARE AND DESIGN SPECIFICATION

3.1. Block Diagram

Systematic steps in the system are shown in the block diagram.

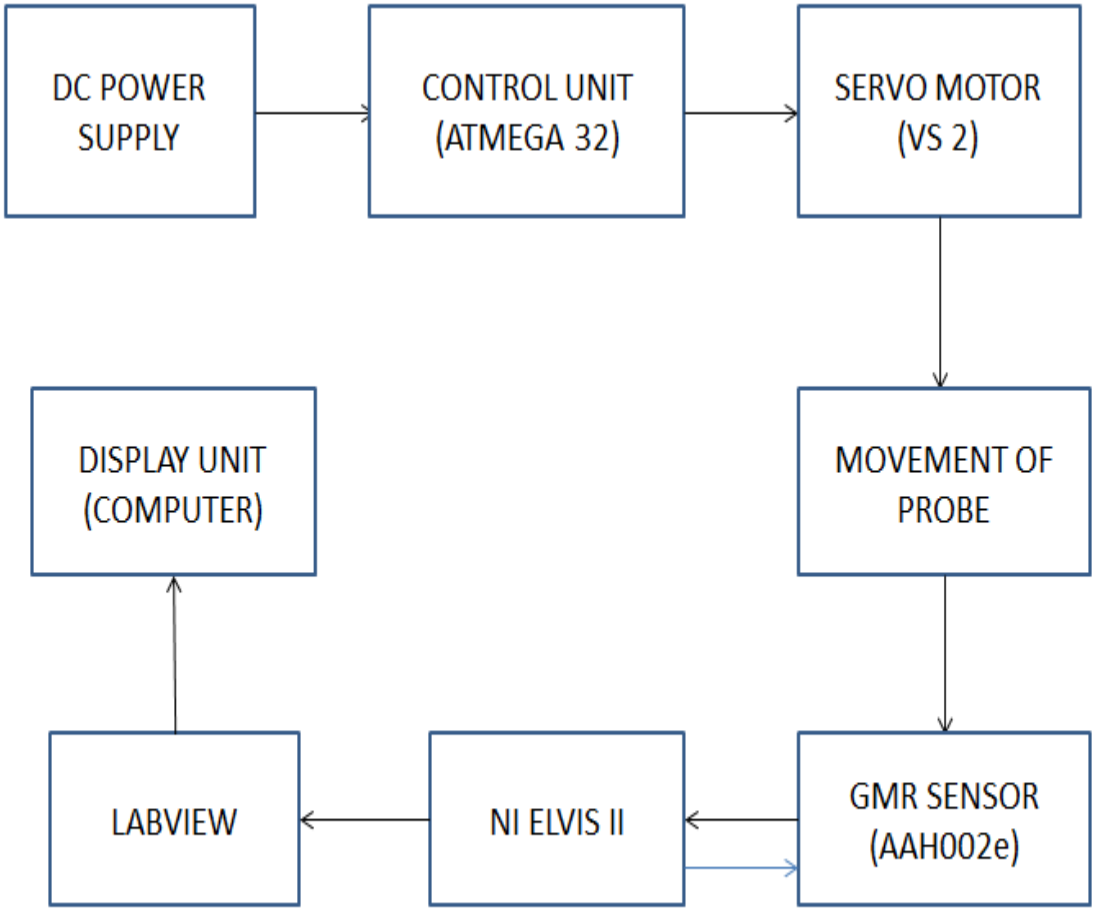

Fig 3.1.1: Block Diagram

3.2. Hardware Selection

3.2.1. GMR Sensor

The term "giant" in giant magnetoresistance (GMR) seems incongruous for a nanotechnology device, it refers to a large change in resistance (typically 10 to 20%) when the devices are subjected to a magnetic field, compared with a maximum sensitivity of a few percent for other types of magnetic sensors.

3.2.1.1 Nanotechnology Structure

GMR structures are ferromagnetic alloys sandwiched around an ultrathin nonmagnetic conducting middle layer: (A) is a conductive, nonmagnetic interlayer. Magnetic moment in alloy (B) layers face opposite directions due to antiferromagnetic coupling. Resistance to current (C) is high. The nonmagnetic conducting layer is often copper. Copper is normally an excellent conductor, but when it is only a few atoms thick, electron scattering causes copper's resistance to increase significantly. This resistance changes depending on the relative orientation of electron spins surrounding the conducting layer.

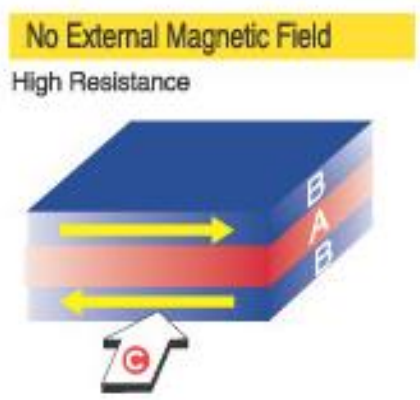

Fig 3.2.1.1(A)

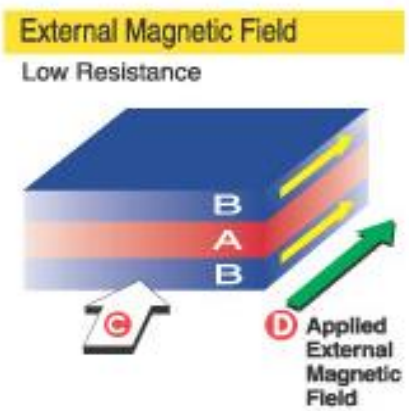

Fig 3.2.1.1(B)

FIG B Applying an external magnetic field (D) overcomes antiferromagnetic coupling, aligning magnetic moments in alloy (B) layers: Such exposure changes the device resistance so the structure can be used to sense an external field. Practical devices are often made of multiple layers of alternating magnetic and nonmagnetic layers to improve sensitivity.

3.2.1.2 The Quantum Mechanics of GMR

To understand how GMR works on the atomic level, consider the following analogies: If a person throws a ball (analogous to a conduction electron) between two sets of rollers turning the same direction (analogous to parallel spin-aligned magnetic layers), the ball tends to go through smoothly. But if the top and bottom rollers turn in opposite directions, the ball tends to bounce and scatter. Alternatively, the GMR effect may be compared to light passing through polarizers. When the polarizers are aligned, light passes through; when their optical axes are rotated with respect to each other, light is blocked.

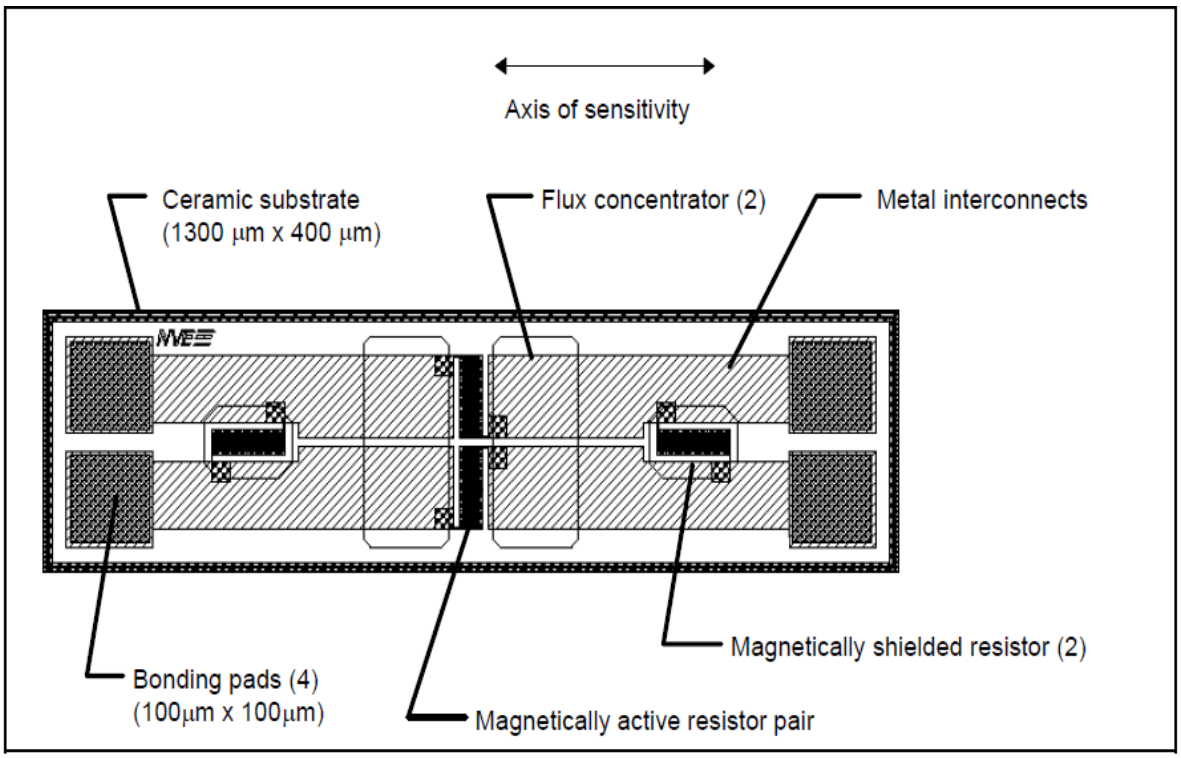

Fig 3.2.1.2: Typical GMR Sensor layout[22]

The resistance of metals depends on the mean free path of their conduction electrons, which, in GMR devices, depends on the spin orientation. In ferromagnetic materials, conduction electrons either spin up when their spin is parallel to the magnetic moment of the ferromagnet, or spin down when they are antiparallel. In nonmagnetic conductors, there are equal numbers of spin-up and spin-down electrons in all energy bands. Because of the ferromagnetic exchange interaction, there is a difference between the number of spin-up and spin-down electrons in the conduction bands. Quantum mechanics dictates that the probability of an electron being scattered when it passes into a ferromagnetic conductor

depends on the direction of its spin. In general, electrons with a spin aligned with the majority of spins in the ferromagnets will travel further without being scattered.

In a GMR spintronic device, the first magnetic layer polarizes the electron spins. The second layer scatters the spins strongly if its moment is not aligned with the polarizer's moment. If the second layer's moment is aligned, it allows the spins to pass. The resistance therefore changes depending on whether the moments of the magnetic layers are parallel (low resistance) or antiparallel (high resistance).

Optimal layer thicknesses enhance magnetic-layer antiparallel coupling, which is necessary to keep the sensor in the high-resistance state when no field is applied. When an external field overcomes the antiparallel coupling, the moments in the magnetic layers align and reduce the resistance. If the layers are not the proper thickness, however, the coupling mechanism can destroy the GMR effect by causing ferromagnetic coupling between the magnetic layers.

For spin-dependent scattering to be a significant part of the total resistance, the layers must be thinner (to a magnitude of several nanometers) than the mean free path of electrons in most spintronic materials. A typical GMR medical sensor has a conducting layer approximately 3 nm (or one ten-millionth of an inch) thick. For reference, that is less than 10 atomic layers of copper, and less than one ten-thousandth the thickness of a piece of tissue paper.

3.2.1.3 Electrical Characteristics

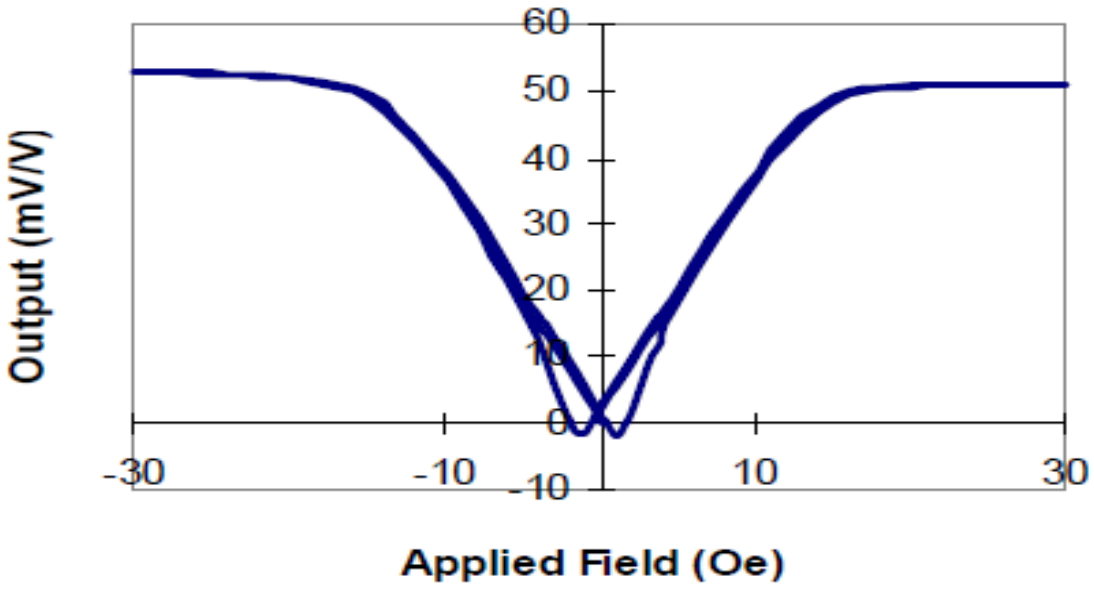

Fig 3.2.1.3 : Electrical characterstics of GMR Sensor[22]

When a magnetic field produces no further change in resistance, it is deemed saturated. The change in resistance from no field to saturation, usually expressed as a percentage of saturated resistance, is known as magnetoresistance. Hysteresis is the separation between positive- and negative-going curves.

Although this diagram shows an omnipolar response, meaning it has the same change in resistance for a directionally positive or directionally negative magnetic field, bipolar sensors have recently become available. Bipolar sensors maintain an operate point with the application of a negative (South) magnetic field, and a release point with the application of a positive (North) magnetic field. The part is ideal for use with magnetic encoders that have alternating North/South pole.

3.2.1.4 AAH002

The AAH002 GMR sensor was manufactured by NVE and was used in this work because of it higher sensitivity comparing with other sensors as shown in Table 1. The AAH002 is one directional GMR and gives analog output with changing the magnetic field.

The AAH-Series GMR sensors are manufactured with a high sensitivity GMR material, making them ideally suited for any low magnetic field application. They are also extremely temperature tolerant, to +150°C operating temperatures. GMR AAH-Series sensors are pure ratiometric devices meaning that they will operate properly at extremely low supply voltages. The output signal will be proportional to the supply voltage. Maximum voltage range is limited by the power dissipation in the package and the maximum operating temperature of the sensor.

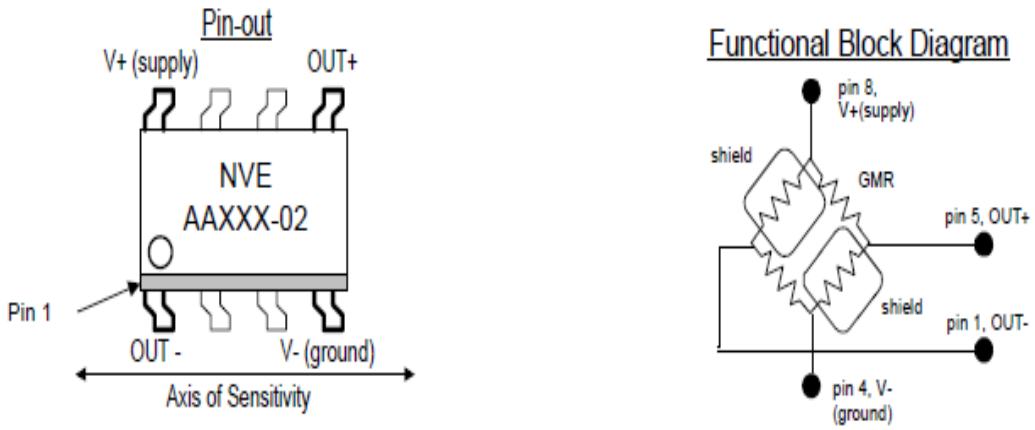

Fig 3.2.1.4.1 : Pin Diagram And Functional Block Diagram Of GMR Sensor[22]

NVE[22] listed some advantages of the one directional .GMR sensor (AAH002) which has excellent sensitivity with wide linear range of operation and DC to > 1 MHz frequency response. GMR sensor is based on Wheatstone bridge which consists of four resistors, two of the four resistors magnetically shielded (inactive) and the other two are active resistors for magnetic field. The sensing axis of the sensor is within the plane of the sample surface. The sensitivity of a GMR bridge sensor can be adjusted in design by changing the lengths of the flux concentrators and the size of the gap between them. The job of these concentrators is to focus the magnetic field on the active resistors and shield the inactive resistors against the applied magnetic field. The goal is to keep the inactive resistors unchanged when the magnetic field is applied. The sensitivity of GMR sensor is related to Signal to Noise ratio (SNR) and lift off between the GMR and the sample under test.

Part Number	Linear Range (|Oe[1]|)		Sensitivity (mV/V-Oe[1])		Maximum Non-linearity (% Uni.[2])	Maximum Hyster-esis (% Uni.[2])	Maximum Operating Temp (°C)	Typical Resis-tance (Ohms)	Package
	Min	Max	Min	Max					
AA002-02	1.5	10.5	3.0	4.2	2	4	125	5K	SOIC8
AA003-02	2.0	14	2	3.2	2	4	125	5K	SOIC8
AA004-00	5.0	35	0.9	1.3	2	4	125	5K	MSOP8
AA004-02	5.0	35	0.9	1.3	2	4	125	5K	SOIC8
AA005-02	10.0	70	0.45	0.65	2	4	125	5K	SOIC8
AA006-00	5.0	35	0.9	1.3	2	4	125	30K	MSOP8
AA006-02	5.0	35	0.9	1.3	2	4	125	30K	SOIC8
AAH002-02	0.6	3.0	11.0	18.0	6	15	150	2K	SOIC8
AAH004-00	1.5	7.5	3.2	4.8	4	15	150	2K	MSOP8
AAL002-02	1.5	10.5	3.0	4.2	2	2	150	5.5K	SOIC8

Table 3.2.1.4.1 : Comparison of NVE analog sensors from (NVE datasheet)[22]

Features:

• Extremely High Sensitivity to Applied Magnetic Fields.
• Wheatstone Bridge analog Output.
• Temperature Tolerance to 150°C Continuous.
• Near-Zero Voltage Operation.
• DC to >1MHz Frequency Response.
• Small, Low-Profile Surface Mount Packages.

Applications:

• Low Voltage, High Temperature Applications
• Low Field Sensing for Magnetic Media Detection
• Earth's Magnetic Field Detection
• Current Sensing.

3.2.2. NI ELVIS II

The National Instruments Educational Laboratory Virtual Instrumentation Suite II is a computer based design and prototyping environment. NI ELVIS II consists of accustom-designed bench top workstation, a prototyping board, a multifunction data acquisition device, and LabVIEW based virtual instruments . This combination provides an integrated, modular instrumentation platform that has comparable functionality to the DMM, Oscilloscope, Function Generator, and power Supply found on the laboratory workbench.

The NI ELVIS II Workstation can be controlled either vi manual dials on the stations front or through software virtual instruments. The NI ELVIS II software suite contains virtual instruments that enable the NI ELVIS II workstation to perform functions similar to a number of much more expensive instruments.

One can use NI ELVIS II in engineering, physical sciences, and biological sciences laboratories. The suite offers full testing, measurement, and data logging capabilities .The environment consists of the following two components:

1. Bench top hardware workspace for building circuits, shown in Figure 3.2.2.1.

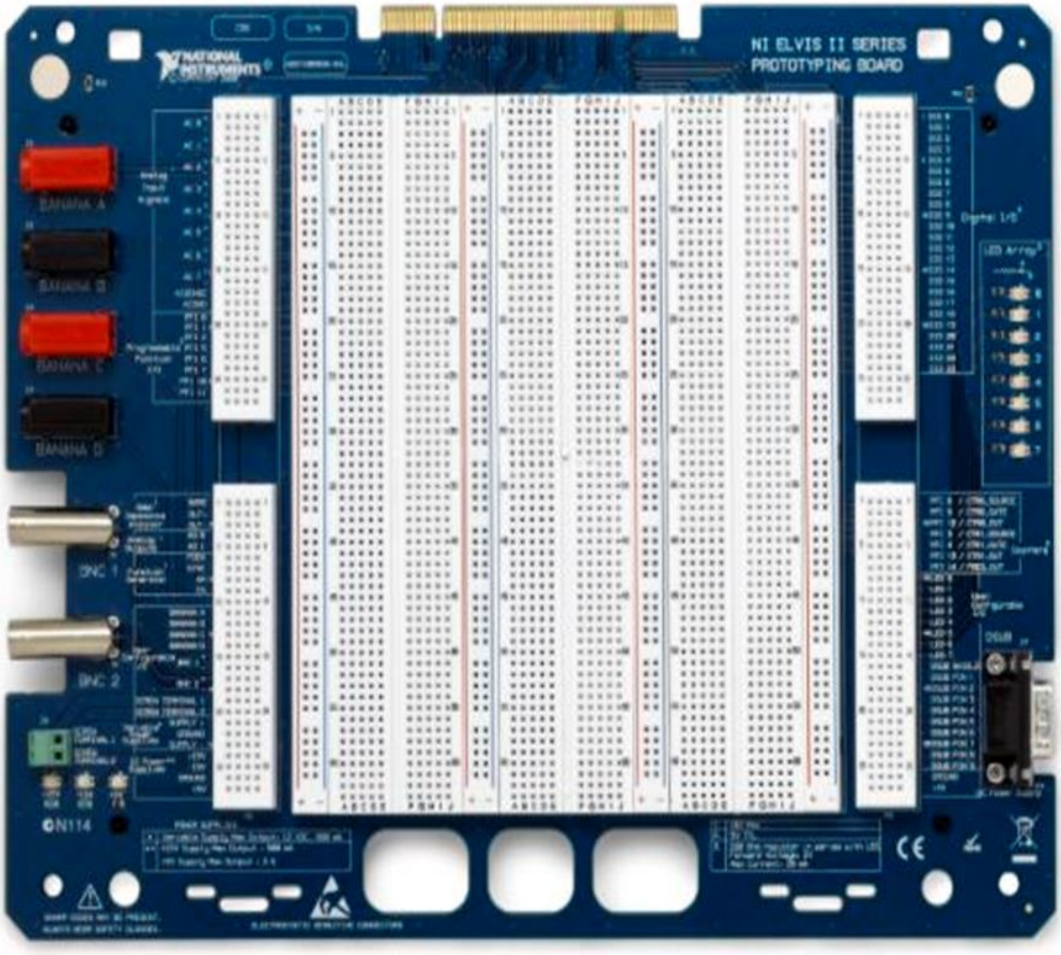

Figure 3.2.2.1: NI ElVIS II hard ware

2. NI Elvis software interface consisting of twelve soft front panels (SFP) instrument, figure 3.2.2.2.

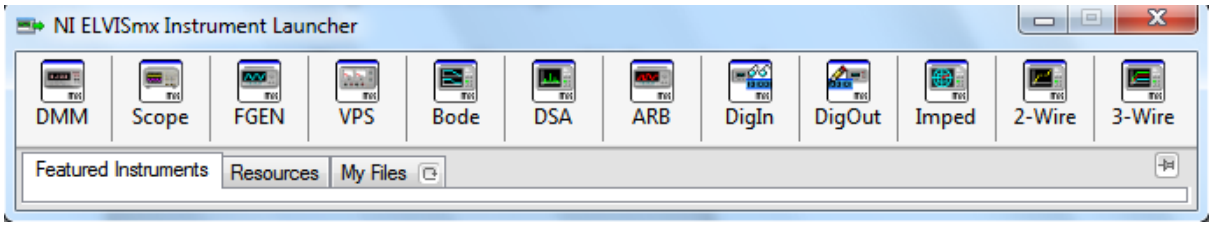

Figure 3.2.2.2: NI ElVIS II Soft Panel

The soft panels are:

• Digital Multimeter (DMM)

• Oscilloscope (Scope)

• Function Generator (FGEN)

• Variable Power Supply (VPS)

• Bode Analyzer

• Dynamic Signal Analyzer (DSA)

• Arbitrary Waveform Generator (ARB)

• Digital Reader (DigIn)

• Digital Writer (DigOut)

• Impedance Analyzer

• Two –wire Current-Voltage Analyzer

• Three –wire Current-Voltage Analyzer

3.2.2.1. Applications

NI ELVIS II SFP instruments, such as the Bode Analyzer and Dynamic Signal Analyzer, offer instructors an opportunity to teach advanced courses in signal analysis and processing.

Students can learn sensor and transducer measurements, in addition to basic circuit design by building custom signal conditioning. They can install custom sensor adapters on the prototyping board. For example, installing a thermocouple jack on the prototyping board allows robust thermocouple connections. The programmable power supply can provide excitation for strain gauges use in strain measurement.

3.2.2.2. NI ELVIS II Bench top Workstation

NI ELVIS II hardware contains Bench top Workstation and Series Prototyping Board The workstation control panel provides easy-to-operate knobs for the variable power supplies and function generator, figure, and offers convenient connectivity and functionality in the form of

BNC and banana-style connectors, shown in figure, to the function generator, scope, and DMM instruments at the right side of the bench top.

3.2.2.3 NI ELVIS II Series Prototyping Board

This section describes the NI ELVIS II Series Prototyping Board and how to use it to connect circuits to NI ELVIS II. The NI ELVIS II Series Prototyping Board connects to the bench top workstation. The prototyping board provides an area for building electronic circuitry and has the necessary connections to access signals for common applications. Figure 3.2.2.3.1 shows the prototyping board with a brief description. You can use multiple prototyping boards interchangeably with the NI ELVIS II Bench top workstation, removing it from the bench top workstation. You can use the prototyping board connector to install custom prototype boards you develop. This connector is mechanically the same as a standard PCI connector.

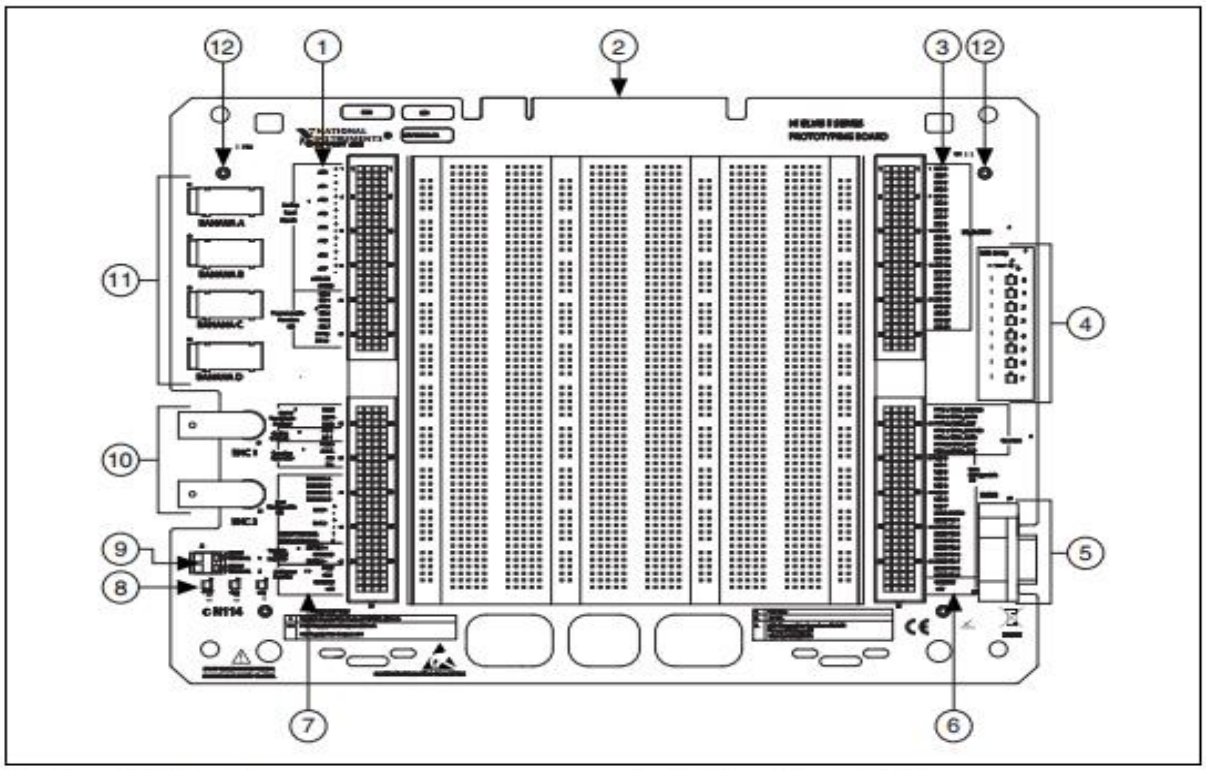

1 AI and PFI Signal Rows
2 Workstation Interface Connector
3 DIO Signal Rows
4 User Configurable LEDs
5 User Configurable D-SUB Connector
6 Counter/Timer, User-Configurable I/O, and DC Power Supply Signal Rows
7 DMM, AO, Function Generator, User-Configurable I/O, Variable Power Supplies, and DC Power Supplies Signal Rows
8 DC Power Supply Indicators
9 User-Configurable Screw Terminals
10 User Configurable BNC Connectors
11 User Configurable Banana Jack Connectors
12 Screw Positions for Locking

Figure 3.2.2.3.1: Prototype Board Description[23]

3.2.2.4. NI ELVIS Functions.

NI ELVIS II performs functions similar to a number of real instruments, which are used in common labs. ELVIS hardware and software integrated to gather to serve multi function as described below.

DMM

The primary DMM instrument on NI ELVIS II is isolated and its terminals are the three banana jacks on the side of the bench top workstation. For DC Voltage, AC and COM voltage, Resistance, Diode, and Continuity Test modes, use the V connectors. For DC Current and AC Current modes, use the A and COM connectors [23]. For easy access to circuits on the prototyping board, you can use banana-to-banana cables to wrap the signals from the user-configurable banana jacks to the DMM connectors on the bench top workstation.

Oscilloscope

The two oscilloscope channels are available at BNC connectors on the side of the input impedance and can bench top workstation. These channels have robust 1 M be used with 1X / 10X attenuated probes. You can also use high-impedance Analog Input channels AI to AI7 available on the prototyping board.

Function Generator (FGEN)

The function generator output can be routed to either the FGEN/TRIG BNC connector or the FGEN terminal on the prototyping board. A +5 V digital signal is available at the SYNC terminal. The AM and FM terminals provide analog inputs for the amplitude and frequency modulation of the function generator output [23].

Power Supplies

The DC power supplies provide fixed output of +15 V, –15 V, and +5 V. The variable power supplies provide adjustable output voltages from 0 to +12 V on the supply+ terminal, and 0 to –12 V on the supply– terminal .All power supplies on NI ELVIS II are referenced to ground [23].

Bode Analyzer

The Bode Analyzer uses the Function Generator to output a stimulus and then uses analog input channels AI 0 and AI 1 to measure the response and stimulus respectively.

3.2.3 Introduction to LabVIEW

LabVIEW (short for Laboratory Virtual Instrumentation Engineering Workbench) is a platform and development environment for a visual programming language from National Instruments. The graphical language is named "G". Originally released for the Apple Macintosh in 1986, LabVIEW is commonly used for data acquisition, instrument control, and industrial automation on a variety of platforms including Microsoft Windows, various flavors of UNIX, Linux, and Mac OS X.

The code files have the extension ".vi", which is an abbreviation for "Virtual Instrument". LabVIEW offers lots of additional Add-Ons and Toolkits.

3.2.3.1 Dataflow programming

The programming language used in LabVIEW, [20] also referred to as G, is a data flow programming language. Execution is determined by the structure of a graphical block diagram (the LV-source code) on which the programmer connects different function-nodes by drawing wires. These wires propagate variables and any node can execute as soon as all its input data become available. Since this might be the case for multiple nodes simultaneously, G is inherently capable of parallel execution. Multi-processing and multi-threading hardware is automatically exploited by the built-in scheduler, which multiplexes multiple OS threads over the nodes ready for execution.

3.2.3.2 Graphical programming

LabVIEW ties the creation of user interfaces (called front panels) into the development cycle. LabVIEW programs/subroutines are called virtual instruments (VIs). Each VI has three components: a block diagram, a front panel, and a connector panel. The last is used to represent the VI in the block diagrams of other, calling VIs. Controls and indicators on the front panel allow an operator to input data into or extract data from a running virtual

instrument. However, the front panel can also serve as a programmatic interface. Thus a virtual instrument can either be run as a program, with the front panel serving as a user interface, or, when dropped as a node onto the blockdiagram, the front panel defines the inputs and outputs for the given node through the connector pane. This implies each VI can be easily tested before being embedded as a subroutine into a larger program. The graphical approach also allows non-programmers to build programs simply by dragging and dropping virtual representations of lab equipment with which they are already familiar. The LabVIEW programming environment, with the included examples and the documentation, makes it simple to create small applications. This is a benefit on one side, but there is also a certain danger of underestimating the expertise needed for good quality "G" programming. For complex algorithms or large-scale code, it is important that the programmer possess an extensive knowledge of the special LabVIEW syntax and the topology of its memory management. The most advanced LabVIEW development systems offer the possibility of building stand-alone applications. Furthermore, it is possible to create distributed applications, which communicate by a client/server scheme, and are therefore easier to implement due to the inherently parallel nature of G-code.

3.2.3.3 Benefits

One benefit of LabVIEW over other development environments is the extensive support for accessing instrumentation hardware. Drivers and abstraction layers for many different types of instruments and buses are included or are available for inclusion. These present themselves as graphical nodes. The abstraction layers offer standard software interfaces to communicate with hardware devices. The provided driver interfaces save program development time. The sales pitch of National Instruments is, therefore, that even people with limited coding experience canwrite programs and deploy test solutions in a reduced time frame when compared to more conventional or competing systems. A new hardware driver topology (DAQmxBase), which consists mainly of G-coded components with only a few register calls through NI Measurement Hardware DDK (Driver Development Kit) functions, provides platform independent hardware access to numerous data acquisition and instrumentation devices. The DAQmxBase driver is available for LabVIEW on Windows, Mac OS X and Linux platforms.

3.2.4. Servo Motor

Here we are using VS 2 SERVO for the linear motion of the probe . Its dimensions are shown in fig .Its features and specifications are as follows:

3.2.4.1 Features

Output Angle : ≥170°

Dead Band Width : 5µsec

Size : 40.6×20.0×38.9 mm(1.6×0.79×1.53in)

Weight : 37 grams

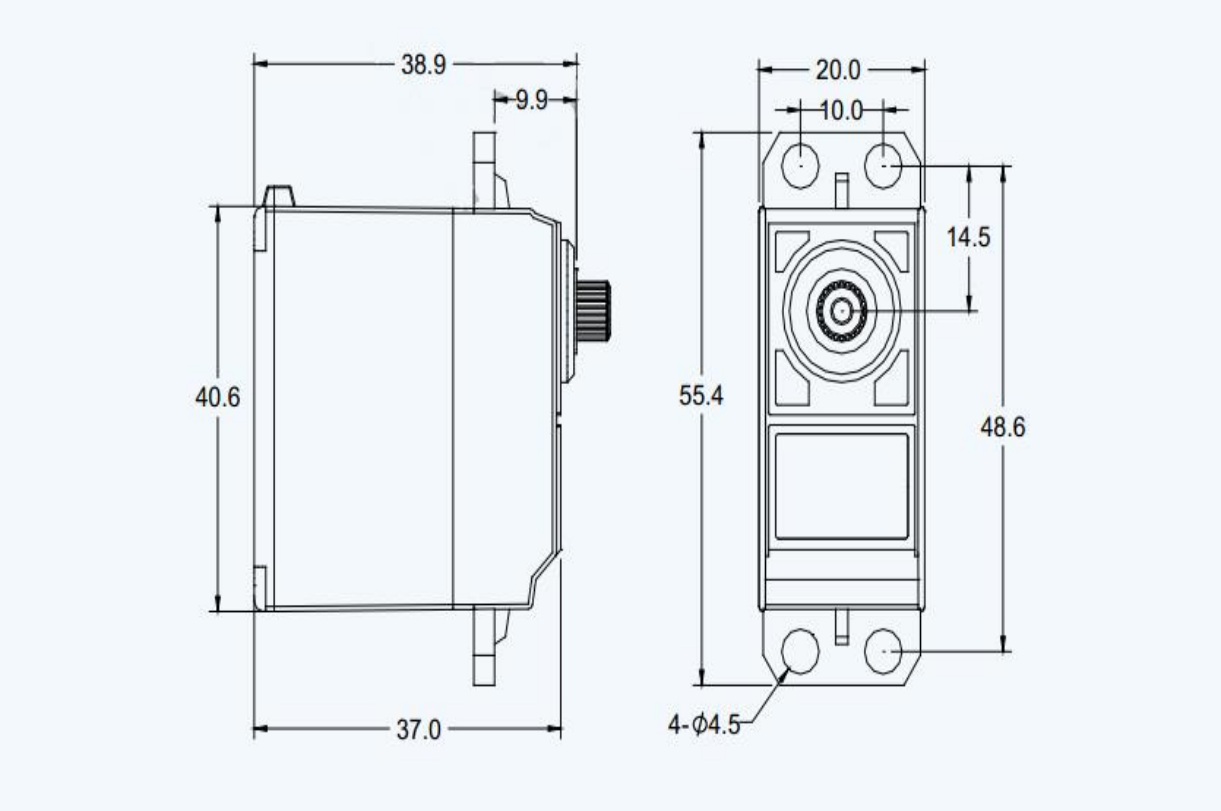

Fig 3.2.4.1.1 : Dimensions Of Servo Motor

3.2.4.2 Technical Data

Control System	Pulse width control, 1500μs neutral	
Operating Voltage	4.8V～6.0V (DC)	
STD Direction	Counter clockwise/pulse traveling 800 to 2200 μs.	
Test Voltage	at 4.8V	at 6.0V
Operating Speed	0.20s/60°at no load	0.17sec/60° at no load
Stall Torque	≥3.2kgf.cm(44.44 oz/in)	≥3.5kgf.cm(48.6 oz/in)
Running Current	～0.2A	～0.25A
Stall Current	～0.8A	～1.0A

Table 3.2.4.2.1 : Technical Data For VS2

3.2.5. Control Unit

The control unit consists of a microcontroller ATmega32 which controls the rotation of motor using pulse width modulated (PWM) wave. It rotates both the motors synchronously using same PWM signal.

The ATmega32 is a low-power CMOS 8-bit microcontroller based on the AVR enhanced RISC architecture. By executing powerful instructions in a single clock cycle, the ATmega32 achieves throughputs approaching 1 MIPS per MHz allowing the system designer to optimize power consumption versus processing speed.

The functional block diagram of timer and counter register is shown in figure 3.2.5.1 .

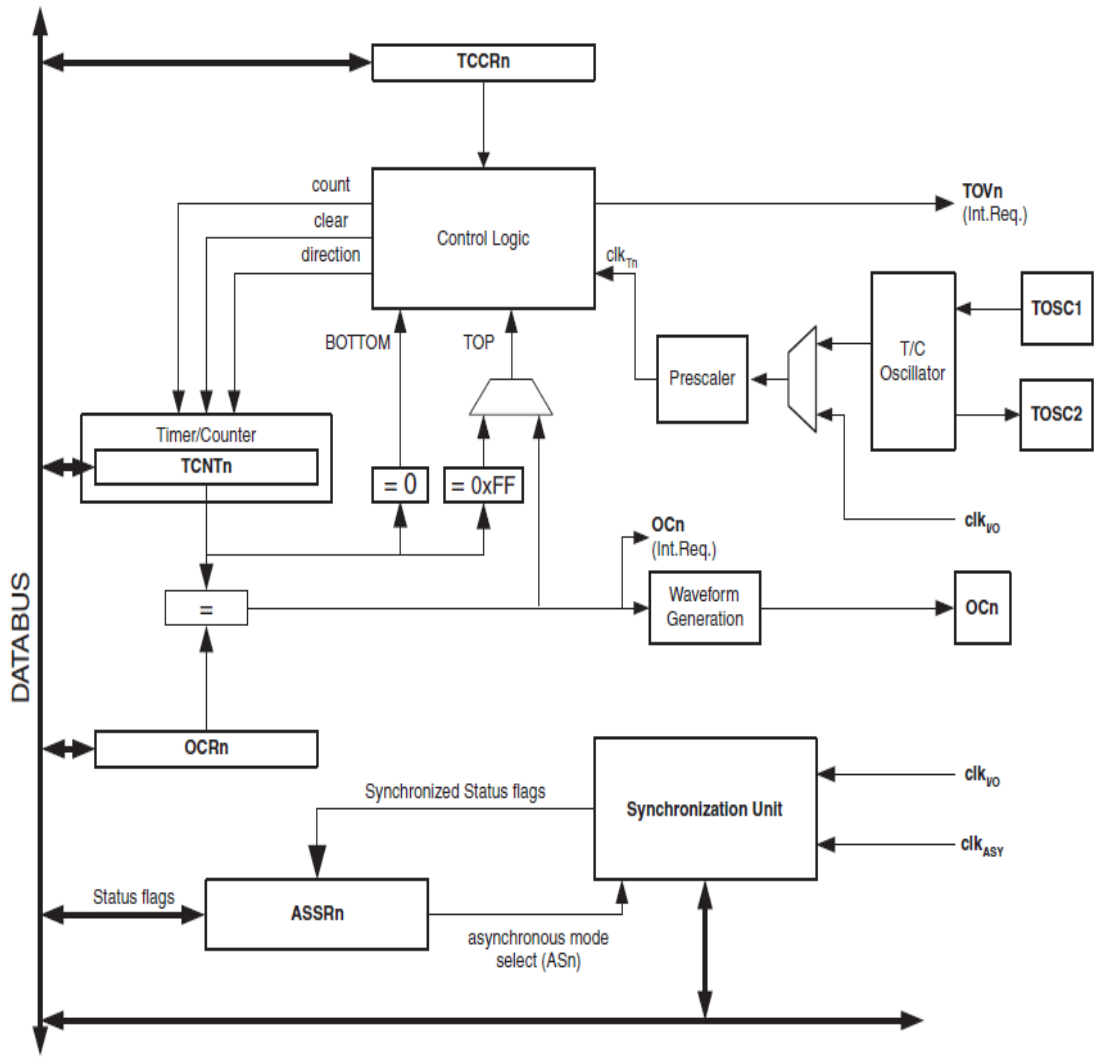

Fig 3.2.5.1 Functional Block Diagram Of Timer And Counter Register

Here we are generating PWM of 250 Hz on pin number 19 ,of desired width and delay with the help of minor changes in timers and counters .The timer/counter control registers(TCCR1A/B) are 8-bit registers and have no CPU access restrictions. Interrupt requests signals are all visible in the Timer Interrupt Flag Register (TIFR). All interrupts are individually masked with the Timer Interrupt Mask Register (TIMSK). TIFR and TIMSK are not shown in the figure since these registers are shared by other timer units. Registers. Instructions used in programming are as follows:

1. TCCR1A

Bit	7	6	5	4	3	2	1	0	
	COM1A1	COM1A0	COM1B1	COM1B0	FOC1A	FOC1B	WGM11	WGM10	TCCR1A
Read/Write	R/W	R/W	R/W	R/W	W	W	R/W	R/W	
Initial Value	0	0	0	0	0	0	0	0	

2. TCCR1B : The noise canceler is enabled by setting the Input Capture Noise Canceler (ICNC1) bit in Timer/Counter Control Register *B* (TCCR1B).

Bit	7	6	5	4	3	2	1	0	
	ICNC1	ICES1	–	WGM13	WGM12	CS12	CS11	CS10	TCCR1B
Read/Write	R/W	R/W	R	R/W	R/W	R/W	R/W	R/W	
Initial Value	0	0	0	0	0	0	0	0	

3. ICR1 : The Timer/Counter incorporates an Input Capture unit that can capture external events and give them a time-stamp indicating time of occurrence. The external signal indicating an event, or multiple events, can be applied via the ICP1 pin or alternatively, via the Analog Comparator unit.The time-stamps can then be used to calculate frequency, duty-cycle, and other features of the signal applied.

4. OCR1 : The 16-bit comparator continuously compares TCNT1 with the Output Compare Register (OCR1x). If TCNT equals OCR1x the comparator signals a match. A match will set the Output Compare Flag (OCF1x) at the next timer clock cycle. If enabled (OCIE1x = 1), the Output Compare Flag generates an output compare interrupt. The OCF1x Flag is automatically cleared when the interrupt is executed.

5. OC1A – Port D, Bit 5 **:** OC1A, Output Compare Match A output: The PD5 pin can serve as an external output for the Timer/Counter1 Output Compare A. The pin has to be configured as an output (DDD5 set (one)) to serve this function. The OC1A pin is also the output pin for the PWM mode timer function.

3.2.6. Instrumentation Amplifier

The INA129 is low power, general purpose instrumentation amplifier offering excellent accuracy[25]. Gain is set by connecting a single external resistor, R, connected between pins 1 and 8. The equation for calculating gain is given by,

$$G = 1 + \frac{49.4k\Omega}{R}$$

Features

- Low Offset Voltage : 50µV Max
- Low Drift : 0.5µV/C Max
- Low Input Bias Current : 5nA Max
- High CMR : 120db Min
- Inputs Protected To : 40V
- Wide Supply Range : 2.25V to 18V
- Low Quiescent Current : 700µA
- 8-Pin Plastic Dip, So-8 package

Applications

- Bridge Amplifier
- Thermocouple Amplifier
- Rtd Sensor Amplifier
- Medical Instrumentation
- Data Acquisition

CHAPTER 4

EXPERIMENTAL TESTING SYSTEM

This chapter discusses the experimental testing system that is used in this project, including the development of the set up for holding and moving the sensor at a particular height and its signal conditioning circuit.

4.1 Lift Off

The lift off is the distance between the probe (containing GMR sensor) and the surface of the sample under test. The lift off needs to be minimized without touching the surface of the specimen. When the lift off increases, the magnetic field becomes ineffective on the surface, thus it reduces the probe sensitivity. T. Dogaru *et al.* [21] investigated the lift off as a function of GMR amplitude of output signal.

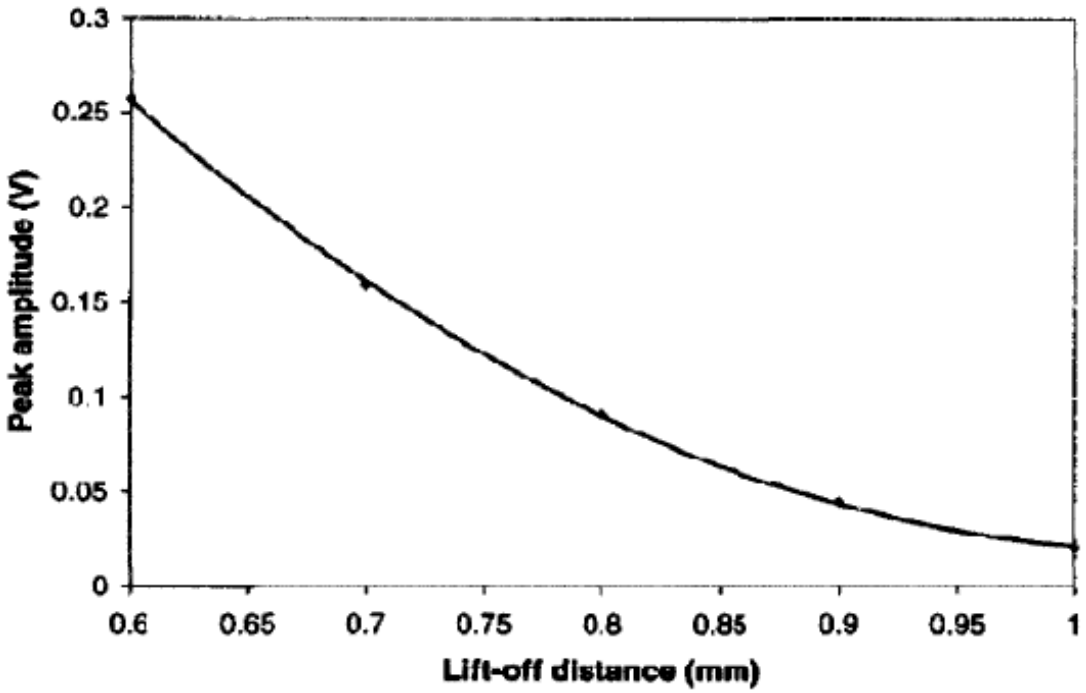

Fig 4.1.1: A peak amplitude as a function of lift off distance between probe and specimen surface by T. Dogaru *et al.* [21]

4.2. System Design

Our objective is to design a system which can hold the probe at the minimum possible height above the sample surface while scanning. Also, it should be able to move the probe at a constant speed without any variation in the lift off between GMR and the sample under test. Another important thing is that the material on which sample will be lying should not affect the magnetic field. Thus a schematic as shown in fig 4.2.1 is designed to keep the sensor moving at a constant height without any change in the lift off between sensor and the sample under the test.

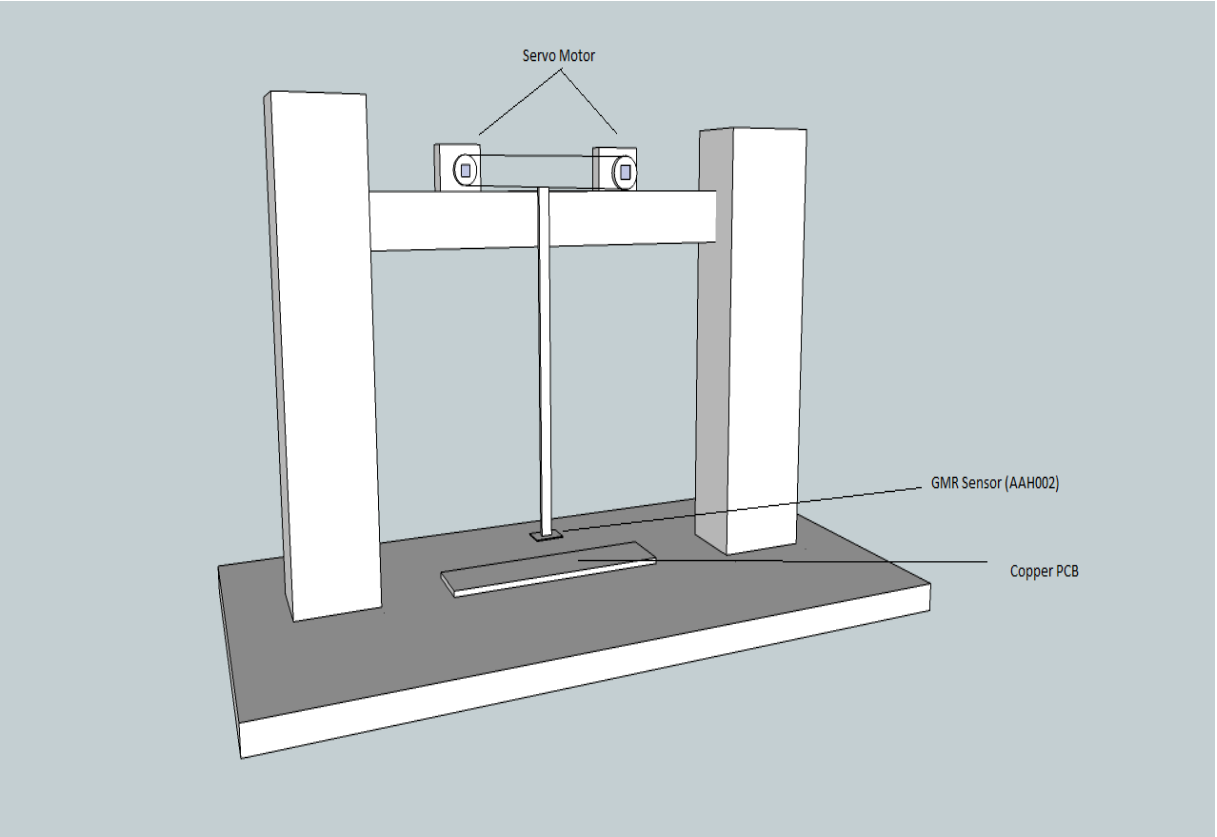

Fig 4.2.1: Schematic of the system designed

4.3. Working of the System Designed

Here we are using two servo motors to move the probe which holds the GMR sensor . These two motors are controlled by a microcontroller (ATMEGA32) .The controller is programmed in such a way that both the motors rotate synchronously using a PWM signal of varying width. The frequency of PWM signal is 250 Hz . The time delay provided is 700ms .The

pulse width are adjusted in such a way that after every 700 ms, it moves of distance of 0.5mm. The following code at pin number 19 is used to generate a PWM signal of 250Hz and required time delay.

```
#include <avr/io.h>

#include <util/delay.h>

int main(void)

{

        int lf,rf,lt,rt,i;

        DDRB |= 0xFF;

        lf=5990;   rf=5920;     lt=99;  rt=94;

        DDRD |= 0xFF;

        //generation of PWMs

        TCCR1A  |=  1<<WGM11  |  1<<COM1A1  |  1<<COM1A0    |  1<<COM1B1  |
1<<COM1B0;

        TCCR1B |= 1<<WGM12 | 1<<WGM13  | 1<<CS10;

        ICR1 = 3999;

        TCCR0  |=  1<<WGM00  |  1<<WGM01  |  1<<CS01  |  1<<CS00  |  0<<COM00  |
1<<COM01;

        TCCR2 |= 1<<WGM20 | 1<<WGM21 | 1<<CS22  | 0<<COM20 | 1<<COM21;

        //OCR1A = ICR1 - 1000;

                OCR1B = ICR1 - 8000;

                  while(1)

                {    for(i=12;i<120;i++)

                {    OCR1A = ICR1 - (i*40);

                _delay_ms(700);

                 }
```

}

}

A path is provided between two metallic strips to keep the movement linear. The metallic strip coming out of this is holding the sensor .The upper part of this strip is attached to the band , which is connecting the gears attached with the two motors. So when the motor rotates this strip moves and the linearity of this motion is assured by the metallic path below the strip. The final set up is shown in fig 4.3.1.

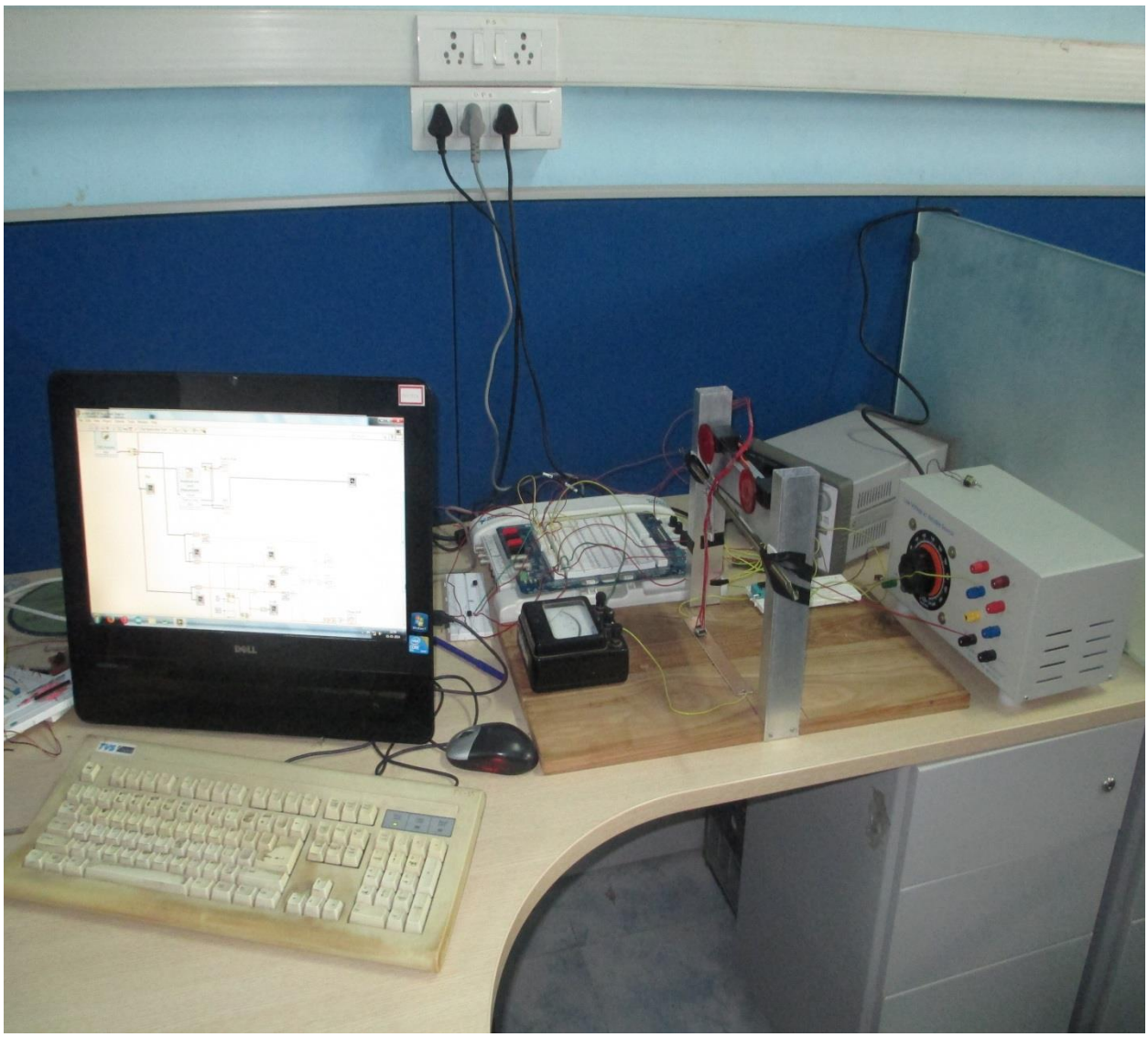

Fig 4.3.1 : Final setup

4.4. Methodology

Tests were performed on PCB (rectangular piece of copper) of dimensions 120mm x12mm as shown in figure 4.4.1. The metal layer in this sample is about 100 Microns in thickness. Two wires were soldered at the two ends of the rectangular PCB. An AC current of magnitude 1A was supplied through these wires to the metal layer of the sample. In the case of injecting AC current experiment, the GMR sensor was used without excitation coil. The AAH002 GMR sensor was manufactured by NVE and was used in this work because of it higher sensitivity comparing with other sensors as shown in Table 1earlier. The AAH002 is one directional GMR and gives analog output with changing the magnetic field. The sensing axis of the sensor is within the plane of the sample surface. The scanning speed of the sensor is 0.4mm/s. The lift off between the sensor and the sample under test is approximately 0.25mm. By injecting AC current on the surface, it creates magnetic field on the conductive material and spreads everywhere on the surface. The 3 mm long scratch on the PCB sample disturbs the magnetic field which can be detected by GMR magnetic sensor. The measurement was performed when the sensitive axis of GMR sensor was parallel to scratch. At the location of scratch there is decrease in output voltage amplitude of the sensor.

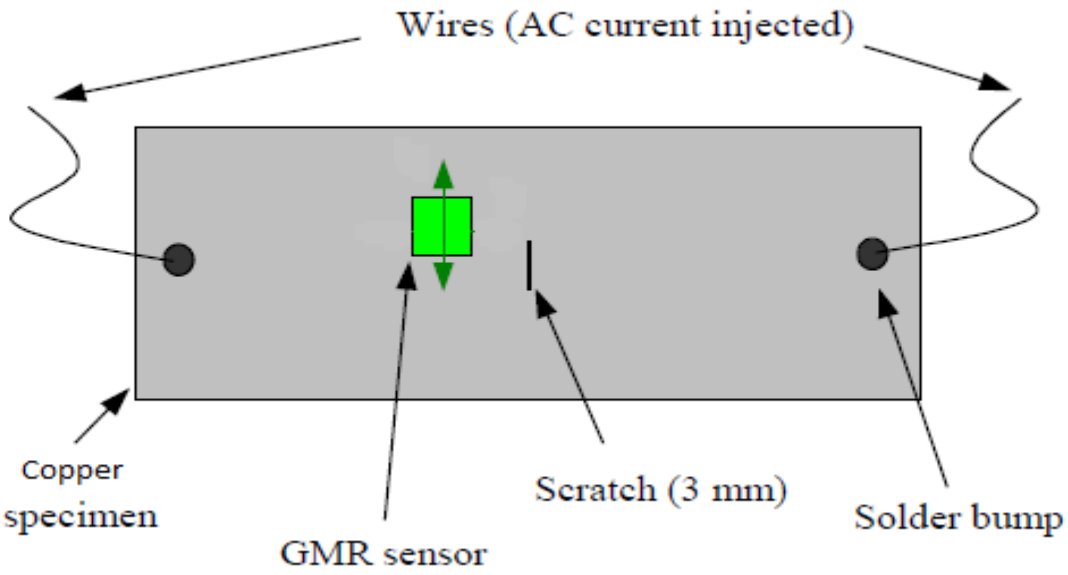

Figure 4.4.1 Schematic Showing The Orientation Of Sensitivity Axis Of The Sensor With Scratch

4.5. Approximation of magnetic field at the sensor element

Here, we calculate the magnetic field strength at the sensor element inside the IC package from a PCB trace with the 1A current. First, we sum the distances between the center of the current-carrying conductor and the sensor element as shown in Figure 1

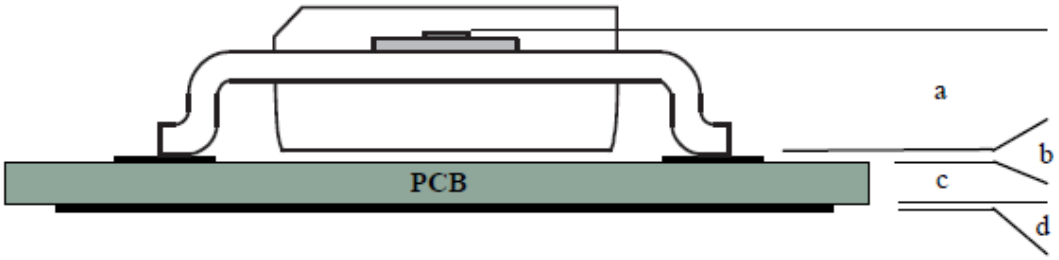

Fig 4.5.1: Distance from the sensor element to the center of the trace[26]

Where,

a = Distance between bottom of leads and the sensor element (specified by NVE).

b = Distance between bottom of package leads and top of PCB.

c = PCB thickness.

d = Distance between bottom of PCB and half trace thickness.

r = Distance of the centre of the trace to the sensor element.

For NVE MSOPs, a = 0.89 mm; for SOIC packages, a = 1.15 mm. The larger SOIC package dimensions make the design less sensitive to mechanical tolerances . Here we are using SOIC. For standard PCBs, copper thickness is 35 μm per ounce plus approximately 20 μm of plating, so b = 125 μm for 3 oz plated copper. The distance to the centre of the conductor is half the trace thickness, so d = 62 μm. Trace thickness is usually negligible for 1 oz copper. We will assume a standard 1.6 mm thick PCB, so:

r = a + b + c + d

= 1.15 mm + 0.125 mm + 1.6 mm + 0.062 mm

= 2.94 mm.

The tolerance in PCB thickness (typically ±10%) will cause an increase or decrease in calculated field strength at the sensor. This variation will be extremely small and can be neglected. The axis of magnetic sensitivity is *along* the package. Therefore, the current-carrying conductor must run perpendicular to this axis for maximum sensitivity as shown in Figure 4.5.2:

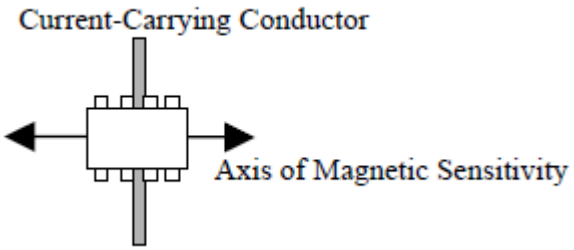

Fig 4.5.2 :Axis Of Magnetic Sensitivity[26]

Using the Biot- Savart Law, the magnetic field at the sensor element is approximated as:

$$H = \frac{I(\cos\theta_A + cos\theta_B)}{4\pi r}$$

Where,

I = current in conductor in amperes,

r = distance of the sensor from the centre of the conductor in meters

H = magnetic field at the sensor element in A/m{SI units(1 A/m = 0.0126 Oe in air)}.

Calculating the magnetic field strength H for our case, where:

- I = 1 A;
- r = 2.94 mm (0.00294 m)
- $D_1 = D_2 = 60$ mm
- $\theta_A = \theta_B = \tan^{-1}(2.94 / 60) = 2.805°$

Therefore,

$$H = \frac{1 (\cos (2.805) + \cos (2.805))}{4 \pi \text{ x } 0.00294}$$

$$= 54.06 \text{ A/m}$$

$$H = 0.681 \text{ Oe}$$

Thus this magnetic field ensures that our sensor is in the linear range of operation as the linear range of our sensor is between 0.6 Oe to 3.0 Oe .

4.6 Signal Conditioning Circuit

The output voltage amplitude of the gmr sensor is amplified by an instrumentation amplifier(INA129P) .The gain of instrumentation amplifier is adjusted to 24 with the help of a single resistor of 2.1kΩ. This amplified output is provided to the input channels of elvis board so that we can monitor the change of output in the real time .The DAQ assistant provides this real time output to the labview so that continuous change in the rms can be monitored and plotted in the waveform chart panel of the labview .To monitor any change in the phase when sensor passes over the scratch, the phase synchronous detector is circuit implemented in the labview. Since, there is no significant change in the phase, its output is not taken into account. The screenshot of the front panel is shown in the fig 4.5.3.The results are discussed in the next chapter.

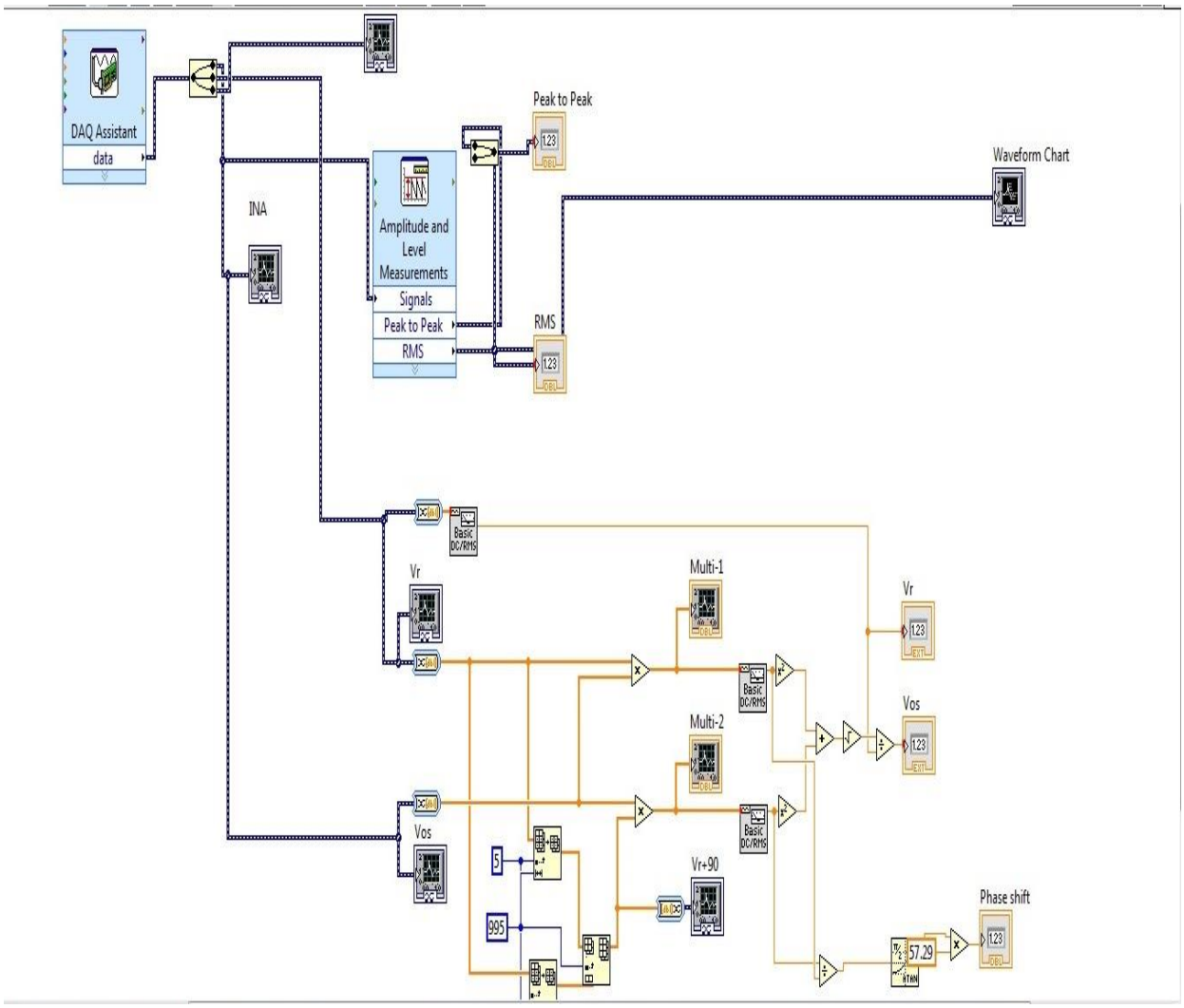

Fig 4.5.3: signal conditioning circuit

CHAPTER 5

RESULTS AND CONCLUSION

5.1 Results

Fig 5.1 (a) and (b) shows the screenshots of the plot of RMS value of the amplified output of the sensor versus the time taken by the sensor to complete scanning .The root mean square value of the amplified output is on X-axis and the time taken by the sensor to scan the surface is on Y-axis.

Fig5.1 (a) shows the plot when there is no scratch on the sample PCB under test .As it can be seen that as the sensor moves over the surface there is no significant change in the RMS value in the specified time interval. There are slight irregularities due to system inaccuracies.

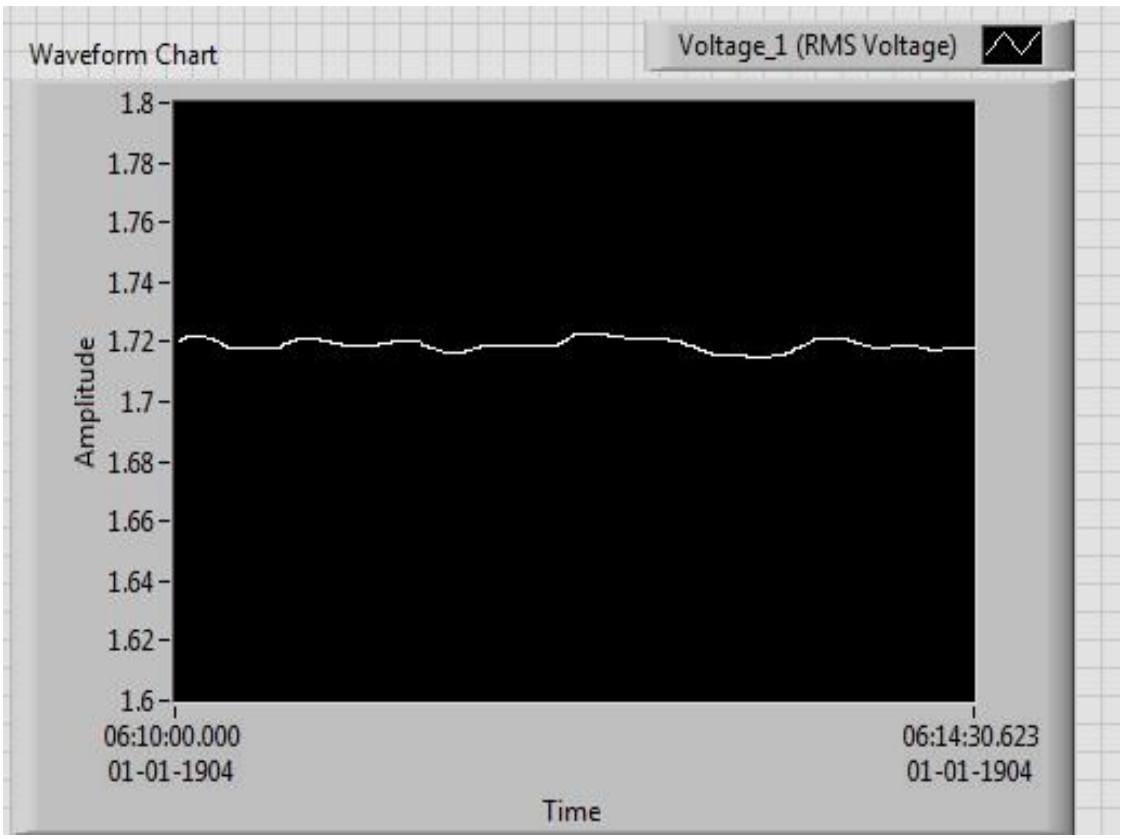

Fig 5.1(a): Output without scratch

Fig5.1 (b) shows the plot when there is scratch of length 3mm and width 0.4 mm on the sample PCB under test .As it can be seen that as the sensor moves over the surface there is no significant change in the RMS value until it reaches the proximity of the scratch. As it reaches near the scratch there is a significant decrease in the RMS .This fall in RMS continues until the sensor reaches exactly over the scratch. Now as the sensor starts moving away from the scratch, the change in RMS increases until it moves away from the proximity of the scratch. After that, it again reaches the level until the scanning is finished .There are slight irregularities in the output due to system inaccuracies.

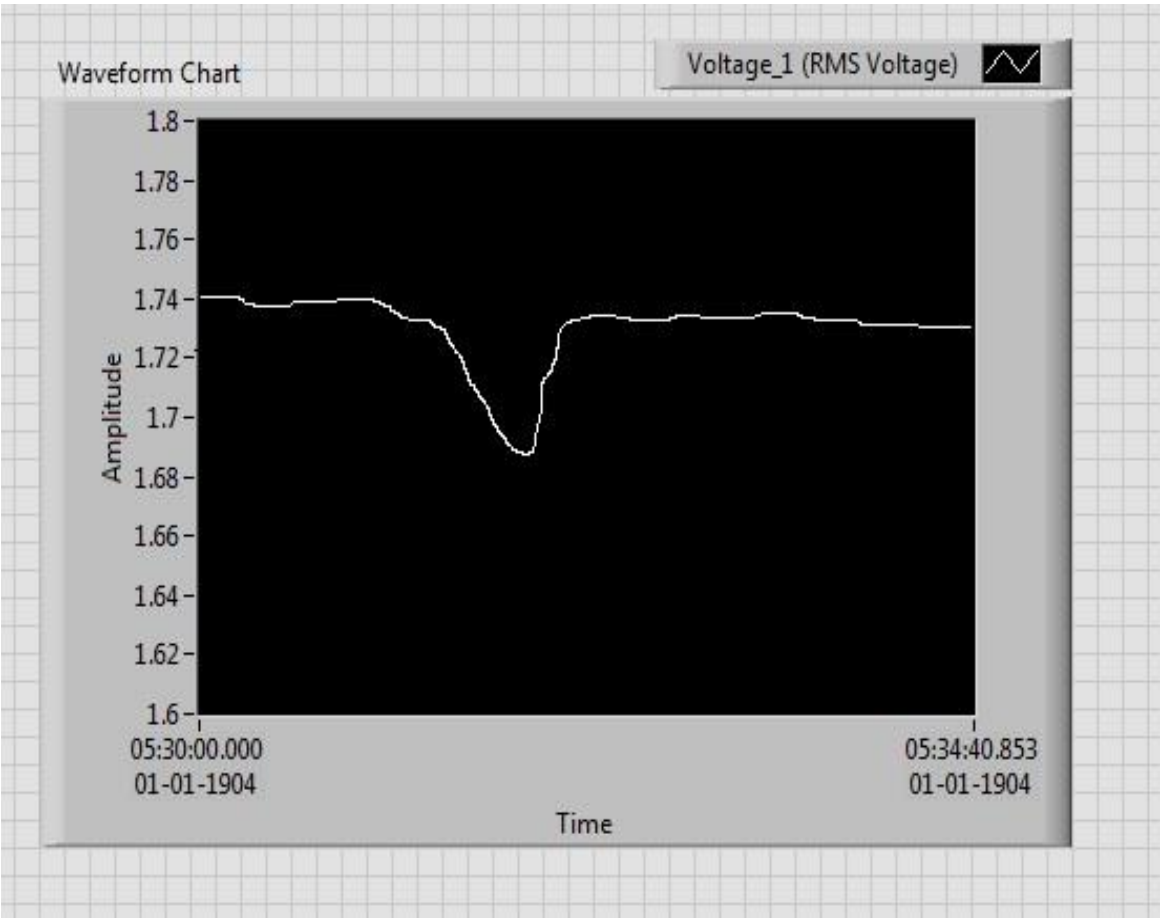

Fig 5.1(b): Output with scratch

The same procedure has been followed with scratches of different width and the difference in voltage from normal level to the lowest level as shown in Fig 4.1(c) has been tabulated in Table I.

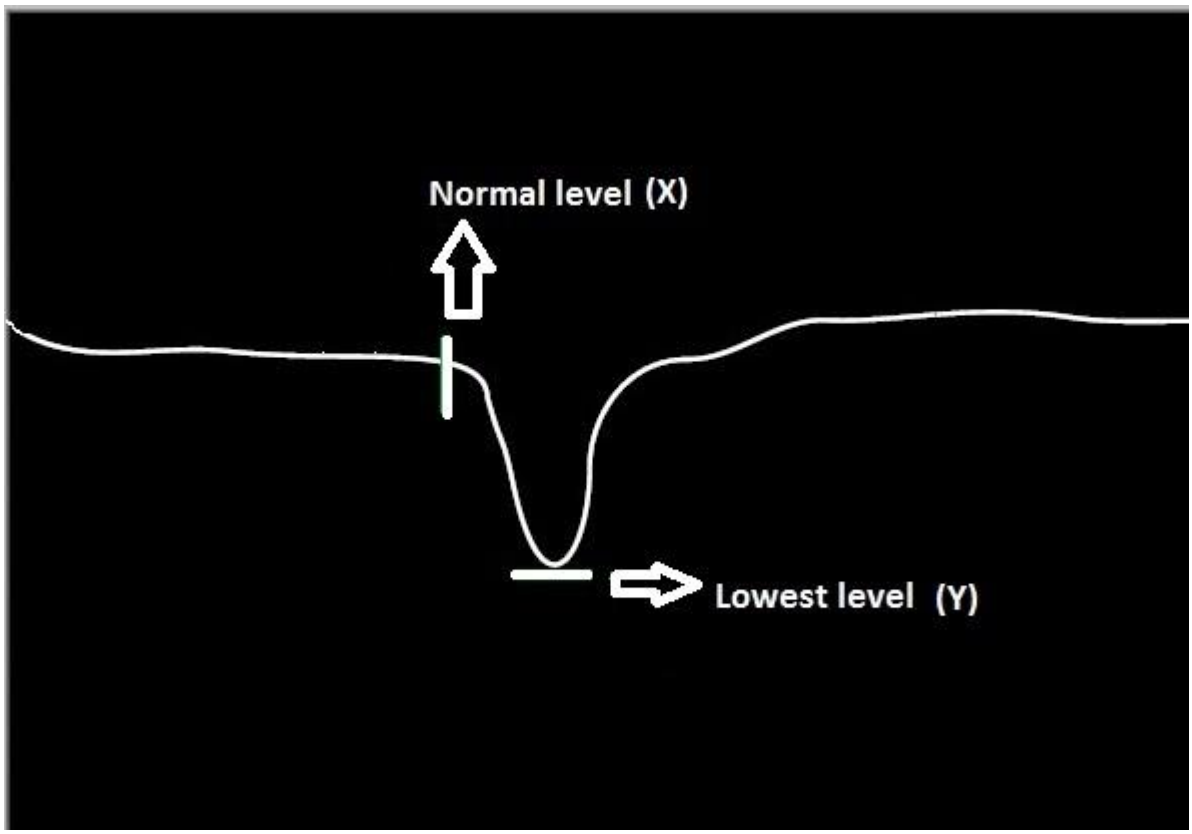

Fig5.1(c) : Figure indicating normal level and lowest level

S.NO	Width of scratch (in mm)	Change in Amplitude (in mV) = X − Y
1	0.400	0 .052
2	0.300	0.041
3	0.200	0.022
4	0.100	0.009

Table 5.1 :values for different width of scratch

Where,

X = rms value at normal level

Y= rms valve at lowest level

Thus with this system it is possible to detect scratch up to the width of 100 micrometers. Below this width, the change in output voltage is not significant.

5.2 Conclusion

The 3 mm long scratch was detected successfully using the GMR magnetic sensor and injecting current. The scratch was created on a rectangular piece of PCB. The PCB dimensions are 120 mm x 20 mm, and the metal layer (copper) in this sample of about 100 microns in thickness. By injecting AC current on the surface, it created magnetic field on the conductive material and spreaded everywhere on the surface. The 3 mm long scratch on the PCB sample disturbs the magnetic field which is detected by GMR magnetic sensor.

It is a non-contact method and can be very useful for detecting defects on the surface or buried under the surface where they are very hard to be detected in visual inspection. The sensor used in this study is very sensitive to small variations of the magnetic field. The AAH002 GMR sensor is used and its orientation is critical issue. For detecting surface defects in metallic layers the orientation of the sensitive axis is coplanar with the surface of the sample.

The sensitivity of this probe depends on the lift-off between the GMR sensor and the sample under test. The lift-off needs to be minimized without touching the surface. The sensitivity of GMR sensor decreases as the lift off between the GMR and the sample under test increases.

CHAPTER 6
FUTURE SCOPE

For future work, the goal is to detect defects of order of hundreds of nanometers in thin conductive surface . Another task will be to increase the scanning speed and to detect small defects in tens of micrometers .Another possiblity is that it can be developed in a pen size structure in such a way that by just moving the pen over the thin conductive surface we will be able to detect defects of the order of micrometers.

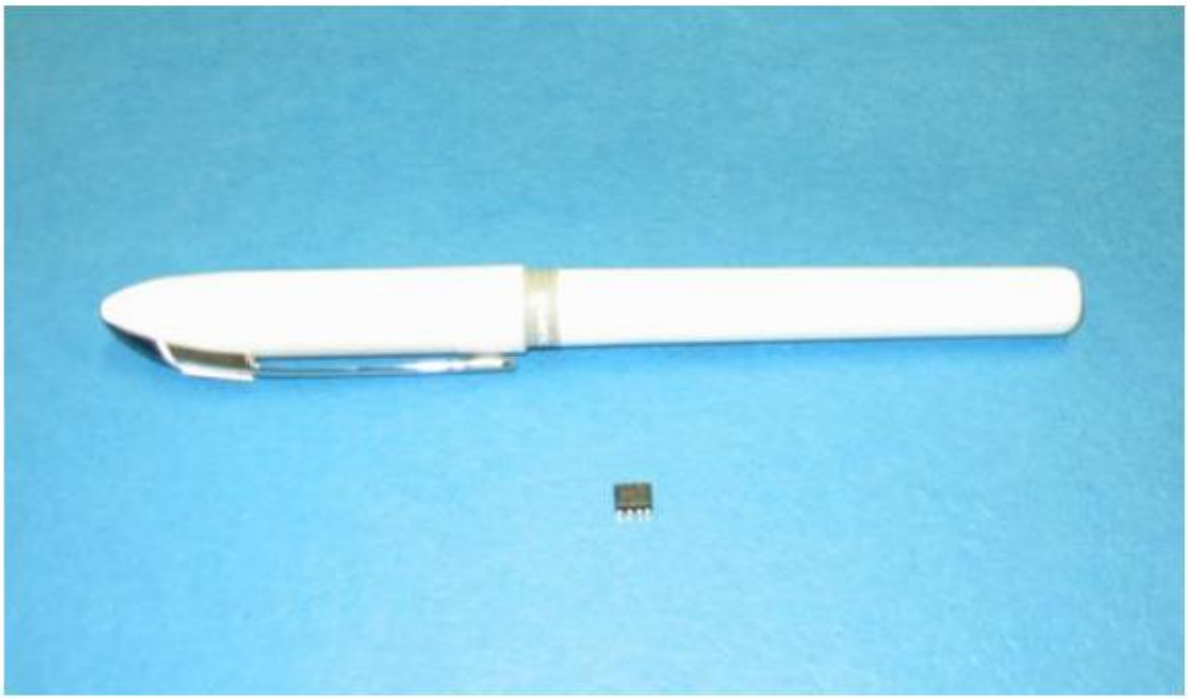

Fig 6.1: Future Scope

REFERENCES

[1] W.H. Hayt, J.A.Buck "Engineering Electromagnetic" McGraw Hill, Chapter 9, seven edition ,2006.

[2] Ed.Ramsden ,"Hall Effect sensors ,Theory Application" Advanstar communication Inc 2001

[3] Paul Emerald. "Low Duty Cycle Operation of Hall Effect Sensors for Circuit Power Conservation" Sensors, Vol. 15, No 3:38 March 1998.

[4] P. Ciureanu and S. Middelhoek. "Thin Film Resistive Sensors", New York: Institute of Physics Publishing. 1992

[5] J.E.Lenz et al. "A Highly Sensitive Magnetoresistive Sensor" iVocSolid State Sensor and Actuator Workshop. 1992.

[6] W.Thomson, "On the electrodynamic qualities of metals: effects of magnetization on the electric conductivity of nickel and iron," Proc.Roy.Soc.London,vol.8, pp. 546-550,1857.

[7] P. Ripka, M. Tondra, R.S Beech, J. Stokes, Eurosensors XII, 1998, Proc. pp.967-969.

[8] T.H. Casselman and S.A. Hanka, Calculation of the performance of a magnetoresistive permalloy magnetic field sensor, IEEE Trans. Magnetics, MAG-16, 461^464, 1980.

[9] P. Mlejnek, M. Vopalensky, P. Ripka. "AMR current measurement device" Sensors and Actuators A: Phys. (2007)

[10] P. Ripka, M. Vopalensky, A. Platil, M. Doscher, K.-M.H. Lenssen, H. Hauser." AMR magnetometer" Journal of Magnetism and Magnetic Materials 254-255 (2003) 639-641.

[11] M. Julliere, Phys. Lett.A 54 (1975)225 ; M. Julliere, Thesis of Rennes University, No. B368/217,Rennes, 197.

[12] M.N. Baibich, J.M.Broto, A.Fert, F. Nguyen Van Dau, and F. Petroff "Giant magneto

resistance of(001) Fe/(001)Cr magnetic Superlattices" Physical Review Letters, Volume 61, Number 21, pp 2472-2475 (1988)

[13] B. Dieny, V. S. Speriosu, B. A. Gurney, S. S. P. Parkin, D. R. Wilhoit, K. P. Roche, S. Metin, D. T. Peterson and S. Nadimi "Spin-valve effect in soft ferromagnetic sandwiches" Journal of Magnetism and Magnetic Materials, Volume 93, February 1991, Pages 101-104

[14] G.A. Prinz "Magnetoelectronics" Science 282: 1660-1663, 27 Nov 1998.

[15] J. Daughton, J.Brown, E.Chen, R.Beech, A.Pohm, and W.Kude "Magnetic Field Sensors Using GMR Multilayer" IEEE Transactions on Magnetic, VOL, 30, NO.6, November 1994.

[16] Nathan A. Stutzke ,Stephen E. Russek, and David P. Pappas "Low-frequency noise measurements on commercial magnetoresistive magnetic field sensors" JOURNAL OF APPLIED PHYSICS 97, 10Q107 (2005)

[17] Hidefumi Yamamoto and Kazuhiko Yamada "The application of giant MR films to magnetic devices" Materials Science and Engineering B, Volume 31, Issues 1-2, April 1995, Pages 207-211

[18] C. Fermon, M. Pannetier-Lecoeur, N. Biziere and B. Cousin "Optimised GMR Sensors for low and high frequencies applications" Sensors and Actuators A: Physical,Volume 129, Issues 1-2, 24 May 2006, Pages 203-206

[19] Carl H. Smith and Robert W. Schneider, "GMR and SDT Sensors and Arrays for Low-Field Magnetic Applications", NVE Corporation

[20] L.K. Wells, "LabVIEW Student Edition User's Guide", National Instruments, 1995.

[21] Teodor Dogaru and Stuart T. Smith "Giant Magnetoresistance-Based Eddy-Current

Sensor "IEEE TRANSACTIONS ON MAGNETICS, VOL. 37, NO. 5, SEPTEMBER 2001.

[22] www.nve.com

[23] http://india.ni.com/

[24] www.atmel.in/Images/doc2503.pdf

[25] instrumentation.obs.carnegiescience.edu/ccd/parts/INA128.pdf

[26]http://www.nve.com/Downloads/SB-SA- 001_Current_Measurement.pdf